Visceral Fat Inflammation and Fat Embolism are associated with Lung's Lipidic Hyaline Membranes in COVID-19 patients

A Cross-sectional, Case-Control Study

PhD in Human Health

XXXIV Cycle

Dottorando

Georgia Colleluori

Docente Tutor

Prof. Giorgio Barbatelli

Correlatori

Prof. Saverio Cinti

Prof. Antonio Giordano

Abstract

Background: Visceral obesity is a critical determinant of severe coronavirus disease-2019 (COVID-19). Methods: In this study, we performed a comprehensive histomorphologic analysis of autoptic visceral adipose tissues (VAT), lungs and livers of 19 COVID-19 and 23 non-COVID-19 subjects. Results: Although there were no between-groups differences in body-mass-index and adipocytes size, higher prevalence of CD68+ macrophages in COVID-19 subjects' VAT was detected ($p=0.005$) and accompanied by crown-like structures presence, signs of adipocytes stress and death. Consistently, human adipocytes were successfully infected by SARS-CoV-2 *in vitro* and displayed lower cell viability. Being VAT inflammation associated with lipids spill-over from dead adipocytes, we studied lipids distribution employing Oil-Red-O staining (ORO). Lipids were observed within lungs and livers interstitial spaces, macrophages, endothelial cells, and vessels' lumen, features suggestive of fat embolism syndrome, more prevalent among COVID-19 individuals ($p<0.001$). Notably, signs of fat embolism were more prevalent among obese ($p=0.03$) independently of COVID-19 diagnosis, suggesting that such condition may be an obesity complication, exacerbated by SARS-CoV-2 infection. Importantly, all infected subjects' lungs presented lipids-rich (ORO+) hyaline membranes, formations associated with COVID-19-related pneumonia, present only in one control with non-COVID-19 pneumonia. Conclusions: This study describes for the first time novel COVID-19-related features possibly underlying the unfavorable prognosis in obese SARS-CoV-2-infected-subjects.

Introduction

SARS-CoV-2 and COVID-19

In December 2019, the novel severe acute respiratory syndrome coronavirus 2 (SARS-CoV-2) was identified for the first time in a cluster of patients with pneumonia of unknown cause belonging to the province Hubei, specifically from the city of Wuhan (1). Since then, SARS-CoV-2 has spread globally resulting in a worldwide health crisis which caused over four million deaths (2). SARS-CoV-2 infection is in fact responsible of the coronavirus disease 2019 (COVID-19), a condition that develops in 5-20% of infected cases (1-5). The SARS-CoV-2-infection clinical spectrum appears in fact to be extremely wide: it may result in asymptomatic cases, mild upper respiratory symptoms, or severe viral pneumonia, respiratory failure, and death (3). Among hospitalized patients, the most commons symptoms at admission are fever, caught, respiratory distress and fatigue (4, 5). A study from the Chinese Center for Disease Control and Prevention involving 72,314 subjects, reported the epidemiological characteristics of the COVID-19 outbreak in China and classified most cases (81%) as mild (non/mild pneumonia), 14% of cases as severe (dyspnea, respiratory frequency ≥ 30/min, blood oxygen saturation ≤93%, partial pressure of arterial oxygen to fraction of inspired oxygen ratio<300 and/or lungs infiltrates >50% within 24-48 hours), and 5% of them as critical (respiratory failure, septic shock, multiple organ dysfunction or failure) (6). These data were published in February 2020 and documented a 2.3% case-fatality rate (6). A similar mortality rate (2.1%) is observed in the worldwide population, data constantly updated by the Coronavirus Resource Center of the Johns Hopkins University (2). However, when the analyses are performed within specific age groups, the mortality rate dramatically changes with subjects with age ≥80 and 70-79 years having a case-fatality ratio of 14.8% and 8.0%, respectively (6).

SARS-CoV-2 replication is accompanied by a rapid macrophage's activation and an increase in circulating pro-inflammatory cytokines (e.g., TNFα, IL–6, IL-1β), reason for which COVID-19 is characterized by the presence of the so called "cytokine storm" contributing to the multiple organ dysfunction (7). In this context, the lung is a crucial SARS-CoV-2 target organ not only due to the

severe bilateral pneumonia observed in 15-30% of hospitalized patients (8, 9), but also because it is the site from which the infection spreads to blood vessels, heart, gut, brain, and kidneys (10). Published data support signs of inflammation and interstitial fibrosis with alveolar hyaline membrane (HM) formation as the main underlying histopathologic event responsible for pneumonia and acute respiratory syndrome distress (3, 4). The reasons for HM bilateral expression, histogenesis, and sudden clinical appearance during COVID-19 early stages are not completely understood (11).

Furthermore, the severity of COVID-19 is strictly associated with the presence of comorbidities, more frequent with advancing age (12). The most common comorbidities among severe cases are hypertension, followed by type 2 diabetes mellitus (T2DM) and coronary heart diseases which pose infected patients at higher risk of developing COVID-19-related complications (sepsis, respiratory and heart failure, and acute respiratory distress syndrome) (5). Importantly, the listed comorbidities are typically observed in patients suffering from obesity (13, 14). It hence does not surprise that patient with obesity have been listed among the high-priority group for the immunization campaign (Position Statement of the European Association for the Study of Obesity and Società Italiana dell'Obesità). In the following sections obesity pathophysiology and the potential biological basis for its association with the severity of COVID-19 are described.

Obesity pathophysiology

Obesity, defined as a body mass index (BMI)≥30 kg/m^2, is a complex, multifactorial, and relapsing disease (15, 16). Obesity and overweight prevalence is estimated to reach nearly 40% of the adulthood population in numerous countries (*e.g.*, USA, Canada, Australia, UK, and Saudi Arabia) (17) and their incidence is expected to further increase during these coming decades (15, 16, 18). Children with obesity are in fact steeply rising (19), and tend to maintain the disease throughout adulthood (20). For these reasons, obesity is considered as a real pandemic, deeply burdening the global health-care systems (21, 22). Form a pathophysiological standpoint obesity is the result of a chronic-positive energy balance which in turn leads to an excessive accumulation of the excess of

lipids, not only within the adipose organ, but also in other cytotypes, a phenomenon resulting in lipotoxicity and deeply compromising several organs' functions (22, 23). Obesity-induced organ dysfunction impairs whole-body energy homeostatic abilities, hence triggering a vicious cycle at the basis of the relapsing nature of the disease. Therefore, it does not surprise that obesity is a chronic illness associated with over 200 medical complications, including insulin resistance, T2DM, hypertension, cardiovascular events, metabolic syndrome, sleep apnea and certain types of cancers (*e.g.*, breast and colon cancer), and that it represents the fifth leading cause of death worldwide (15, 22).

In obesity, the chronic caloric excess is stored in the form of lipids in the adipose organ which is composed by different compartments: subcutaneous adipose tissue (SAT) and visceral adipose tissue (VAT) which are composed by white adipocytes and form the white adipose tissues (WAT) and by brown adipose tissue (BAT) composed by brown adipocytes (24). Each compartment in turn comprises distinct depots (*e.g.*, for VAT: mesenteric, omental, perirenal etc..) (24). While white adipocyte's main function is to store lipid to supply other organs in moments of starvation, brown adipocytes dissipate energy to produce heat, and play a thermogenetic role (25).

In obesity, the adipose organ expansion interests WAT and occurs through adipocyte hypertrophy and hyperplasia (26). Adipocyte volume in humans is positively related to total fat mass, while adipocyte number is set during adolescence and remains relatively stable throughout life (27, 28). Consistently, adipocyte hypertrophy, but not hyperplasia is observed in healthy adults after 4 months of weight gain (29), while massive weight loss by bariatric surgery results in the reduction of adipocyte size, but not number (27). However, adipocyte hyperplasia has been detected in adulthood, specifically in VAT depots upon sustained positive energy balance, moment at which adipocytes cannot further accommodate the extra calories increasing their size (26, 30). Lipids are in fact first preferentially deposited in SAT, and then, once SAT storage abilities are saturated, they are stored in VAT and ectopic depots (*e.g.,* liver, skeletal muscle, pancreas, heart), a phenomenon representing the

primum movens of lipotoxicity (31). Differently from SAT, VAT and ectopic fat localizations are in fact associated with insulin resistance, T2DM, dyslipidemia, chronic inflammation, and hypertension (32-35), all conditions that, based on clinical observations, increase subjects mortality risk independently of BMI (36-38). The worse metabolic phenotype reported for the so-called *apple-shaped* (high waist-to hip circumference ratio typically observed in men) vs *peer-shaped* adipose tissue distribution is explained by such association (39). SAT adipocyte hypertrophy is correlated with low adipocyte generation rate which in turn predicts insulin resistance in humans and animal models (26, 27, 40, 41). Obesity is in fact characterized by preadipocyte dysfunction and reduced ability to perform *de novo* adipogenesis, a feature contributing to the reduced adipose depot expandability and at the basis of the metabolic anomalies related to the disease (42, 43). SAT adipogenic potential is reduced among prediabetic and diabetic subjects with obesity compared to obese individuals with normal glucose control, while SAT and VAT adipogenic precursors are lower among the first two groups as compared to the last one (44). Collectively, the above data support progressive human WAT dysfunction evident not only comparing normo-weight and obese subjects, but also within the obese population comparing those with different glucose control.

The obesity-associated metabolic anomalies are paradoxically due to the limited adipose organ expandability, hence adipocyte plasticity: adipocytes become hypertrophic until a *critical size* threshold, specific for each depot, is reached; above such threshold cells cannot further expand, display anomalies in fatty acid flux, signs of stress, and die of pyroptosis (45, 46). In this condition, hypertrophic adipocytes are also characterized by alterations in the adipokines and chemokine expression pattern (*i.e.*, lower adiponectin, higher TNFα, IL-6, MCP1 and resistin), which in turn attract pro-inflammatory immune cells, resulting in chronic, low-grade inflammation and insulin resistance (46, 47). Accordingly, a particular adipocyte size threshold associated with T2DM and low metabolic response to gastric bypass was identified in patients suffering from obesity (48). Adipocyte's stress and death is hence accompanied by inflammatory cells infiltration: pro-inflammatory macrophages absorb cell remnants/debris and surround dead adipocytes forming the

so-called *crown like structures* (-CLS- Figure 3) (45, 49). Hence, it is not surprising that CLS are more prevalent in obese than normo-weight subjects (45) and that their presence in the adipose tissue is associated with lower insulin sensitivity, higher VAT size, ectopic fat infiltration (liver and muscle) and circulating inflammatory cytokines (*e.g.*, TNFα; IL6) (50). Importantly, the strong association between visceral obesity and insulin resistance may be in part explained by the lower *critical death size* of visceral adipocytes, which therefore display lower plasticity and tissue remodeling abilities compared to the ones belonging to SAT depots (46, 49). In addition, as VAT discharges the free fatty acids excess directly into the portal circulation, liver fat accumulation is observed in condition of visceral obesity and often results in the *non-alcoholic fatty liver steatohepatatis* (NASH) also associated with liver dysfunction and insulin resistance (14). Circulating free fatty acids then reach the skeletal muscle leading to tissue inflammation and dysfunction, strongly contributing to systemic insulin resistance (51). Furthermore, pancreatic lipids deposition in condition of chronic positive energy balance also occurs and deeply compromises β cell function, hence glucose tolerance (52). Based on the above phenomena, the beneficial effects of PPARγ agonists (thiazolidinediones), drugs able to reduce circulating free fatty acids increasing adipose expandability, for the treatment of T2DM are not surprising (53). Adipocyte's hypertrophy is also related to tissue remodeling anomalies such as insufficient angiogenesis, fibrosis, and hypoxia, all phenomena responsible for reduced tissue plasticity and functional alterations (54-56). Adipose tissue fibrosis in fact predicts response to Roux-en-Y Gastric Bypass with the higher fibrosis being associated to poorer weight loss response (57). Clément's group demonstrated that obesity is characterized by an increased WAT prevalence of a subpopulation of collagen producing PDGRFα+ adipose precursors which may act synergistically with the increased TGFβ levels leading to WAT fibrosis, local and systemic metabolic alterations (58). It is worth noting that SAT and VAT capillary density is lower among patients with obesity compared to normo-weight individuals, independently of their glycemic control, but that capillary basal membrane was thicker among individuals with prediabetes and T2DM, a feature that may explain the microvascular complications associated with such metabolic anomalies (44).

Aging is associated with fat redistribution in favor of VAT depots (as opposed to subcutaneous) which occurs independently of weight gain (33, 59, 60) and strongly contributes to the age-related cardiometabolic risks (39). While the adipose tissue redistribution occurring with advancing age is partly attributed to sex hormonal profile modifications (61-65), the rise in the relative fat amount is due to multiple factors (14). Importantly, not all adipose depots display the same age-related variations. Brown adipose tissue, for example, reduces with advancing age, partly contributing to the energy expenditure decrease among elderly (66, 67).

Obesity and COVID-19

Obesity, especially severe obesity, is a strong independent risk factor for COVID-19 severity (12) and is associated with higher chance of infection and greater viral load (68-70). While obesity alone is responsible for 20% of COVID-19 hospitalizations, obesity in combination with T2DM and hypertension accounts for 58% (71). Obesity and impaired metabolic health are in fact strongly associated with COVID-19 unfavorable prognosis and pose also young patients at higher risks (72, 73). Importantly, visceral obesity increases the risk of COVID-19-related complications, independently of age, gender, BMI, total and subcutaneous adipose tissue areas (13, 74-76). Visceral obesity is in fact strongly associated with chronic low-grade inflammation, blood hypercoagulability, impaired metabolic health, and higher incidence of cardiovascular events, all risk factors for COVID-19 severity (12, 13, 73, 77, 78). COVID-19 associated cytokine storm, hence elevated inflammatory status, causes multiple organs dysfunction and endothelial alterations, both associated with blood hypercoagulability (7). Furthermore, SARS-CoV-2 infection was demonstrated to be associated with an increase in circulating free fatty acids, in turn contributing for the elevation in circulating inflammatory markers such as IL-6 and CRP (79). SARS-CoV-2 infection in fact mobilizes free fatty acids to support the capsid-associated membrane formation, reason for which COVID-19 is associated with elevated circulating free fatty acids in hospitalized patients with severe pneumonia (80). Importantly, hyperglycemia was also demonstrated to be highly prevalent among intubated

(91.1%) and deceased (72.8%) subjects with COVID-19 in a study conducted on 3,854 patients (81). The same study also reported that the median hospital stay length was more than 2-fold longer among hyperglycemic subjects (10 days) compared to those without hyperglycemia (5 days). Interestingly, COVID-19 severity and hyperglycemia were associated with low circulating adiponectin/leptin ratio (81).

Based on the above evidence, numerous elements and comorbidities are possibly responsible for the strong association between obesity and COVID-19 severity. However, mechanistic analyses specifically focused on the study of the adipose organ among COVID-19 subjects are lacking. Adipocytes ACE2 expression in obesity (82), receptor exploited by SARS-CoV-2 for cell entry, has been often speculated as a possible pathophysiological mechanism responsible for obesity-related COVID-19 severity (12, 83, 84). Similarly, adipocytes express proteases (*e.g., Furin, TMPRSS2*) that may be exploited by SARS-CoV-2 to enter cells (81, 84), and directly infect the adipose organ. Reiterer and colleagues recently demonstrated that SARS-CoV-2 can infect human breast and 3T3L1 adipocytes *in vitro*, last of which displayed reduced *Adiponectin* expression upon infection (81).

In our preliminary study, we observed the presence of fat embolism in a COVID-19 subject with obesity, a phenomenon that we hypothesized could derive from adipose tissue stress induced by SARS-CoV-2 and explain COVID-19 severity in obesity (83). VAT excessive expansion is in fact paralleled by adipocytes hypertrophy, death, and lipids spill-over (14, 45, 85). All those phenomena lead to tissue inflammation and strongly contribute to the obesity-related complications (14, 45, 85). We hence hypothesize that SARS-CoV-2 could directly (infecting adipocytes) or indirectly (causing COVID-19) lead to adipocytes stress, death and lipids release responsible for fat embolism.

Fat embolism

Fat embolism is defined as the presence of lipidic globules within the circulatory system and often occurs without clinical manifestations (86-88). Fat emboli usually accumulate within the microcirculation and have been mainly described in lung (pulmonary emboli) and brain (brain

emboli). Fat emboli may lead to fat embolism syndrome (FES) whose clinical features may comprise respiratory anomalies (shortness of breath, difficulties in breathing), nonspecific neurologic symptoms (*i.e.,* confusion, lethargy, coma) and dermatological symptoms (*i.e.*, petechiae, rush) (87, 88). The main laboratory characteristics of FES is hypoxemia (PaO_2<60 mm/Hg) (88). However, standardized criteria for FES assessment are not available, as its manifestations and laboratory assays are nonspecific. For these reasons its diagnosis is usually one of exclusion (88).

FES has been mainly detected in patients who experienced long bone fractures, even though non-traumatic FES has been also described in specific cases of subjects with hepatocellular carcinoma, bone marrow necrosis, liver steatosis, following the prolonged use of corticosteroids and in additional spare cases (for review see Meng et al., 2020 (87)). Traumatic FES may also occur following intramedullary nailing or liposuction, all procedures that involve the disruption of fat cells (88). Importantly, fat embolism not always results in clinical sequelae, hence FES, reason for which it is considered more frequent than syndrome occurrence. The highest FES incidence was revealed in subjects' victims of traumatic injuries, specifically having long bone or pelvic fractures (up to ~4%) (89). Based on retrospective studies, FES occurs in less than 1% of cases of long bone fractures (89, 90), whereas prospective analyses revealed a higher incidence (86, 88). In a study conducted on autoptic samples obtained from victims of bone fractures, 82% were revealed to have fat emboli, and 33% of those individuals with fat embolism had FES (88). Such discordance may be related to the lack of uniform criteria for FES diagnosis (88).

Two etiologic theories have been formulated to explain fat emboli formation: mechanical and biochemical (88). The mechanical theory, which may apply in condition of traumatic FES, considers the traumatic events involving fat containing tissues *e.g.*, bone marrow and adipose organ, as triggers of fat emboli formation. In these cases, the release of medullary or adipose depot lipids following bone fractures, medullary nailing, liposuction, or other surgical procedure, leads to the formation of fat emboli which enter the circulation and reach lungs, brain, and other tissues (87, 88). On the other side, based on the biochemical hypothesis, fat emboli formation occurs through the aggregation of

lipids in circulation which may be induced by an elevation of the C reactive protein (CRP) whose levels are increased upon inflammation (87, 91, 92). Importantly, free fatty acids also trigger a cascade of thrombotic events that lead to the production of fibrin and platelet aggregation (88, 92).

Interestingly, while our preliminary data revealed the presence of fat emboli in a subject with COVID-19 (83), results from a recent case report documented signs and symptoms similarities between COVID-19 and FES (93). In the context of COVID-19 pandemic, it is hence worth exploring incidence, signs, symptoms, and clinical significance of fat embolism.

Study hypothesis and objective

Based on the above observations, it is possible that in obesity, characterized by the coexistence of chronic low-grade inflammation and dyslipidemia, the excess of lipids in circulation are aggregated to form fat globules, hence fat emboli, and that such phenomenon may be exacerbated by the documented adipocytes death typical of the disease. On the other side, fat emboli formation may also occur due to COVID-19, where not only SARS-CoV-2 triggers the cytokine storm and the free fatty acid increase in circulation, but can also directly infect adipocytes possibly leading to their stress and death. In support of this hypothesis there are our preliminary data (83) and results from a recent case report which documented signs and symptoms similarities of COVID-19 and FES, pointing the attention to the need of performing an accurate differential diagnosis between the two conditions (93). Although obesity has been strongly associated with COVID-19 severity (but not higher infection rates), original articles comprehensively analyzing adipose tissue samples belonging to COVID-19 subjects and providing direct evidence of SARS-CoV-2 infection are lacking (13).

In the present study we perform for the first time a comprehensive histomorphological assessment of visceral adipose tissues, lung, and liver autoptic samples belonging to COVID-19 and non-COVID-19 subjects, specifically focusing on tissues lipids distribution. We observed novel SARS-CoV-2-related histopathological features *i.e.*, visceral adipose tissue inflammation, signs of

fat embolism and lung's hyaline membranes of lipidic nature, possibly contributing to the severity of COVID-19 among subjects with visceral obesity.

Materials and methods

Study Approval

We followed the report "Research ethics during COVID-19 pandemic: observational, and in particular, epidemiological studies" published by the Italian *Istituto Superiore di Sanità* on May 2020 (Rapporto ISS COVID-19, n. 47/2020) (94). Given the observational (cross-sectional, case-control) nature of our study which was conducted on autoptic specimens and did not entail neither an intervention, nor the collection of subject's sensitive information, we have not obtained an informed consent. Our study did not entail any physical risk for the subjects. In Italy, the evaluation of non-pharmacological observational studies is not governed by the same normative references provided for the evaluation of clinical trials and observational studies concerning drugs. Furthermore, as reported in the above report (94) in the section dedicated to our type of study *in conditions of pandemic and therefore of high risk for the communities, some administrative steps may be abolished*. Therefore, our Institutional Review Board does not require an ethical approval for studies conducted on autoptic specimens and not collecting personal or sensitive data.

Study subjects and tissue sampling

Autoptic lung, liver, and visceral adipose tissue samples of 49 subjects were collected at the Department of Legal Medicine of the Ospedali Riuniti of Ancona between March 2020 and May 2021. Twenty-four subjects were affected by COVID-19, while the remaining 25 were not and died for different reasons. SARS-CoV-2 infection was assessed in all subjects by RT-PCR tests on nasopharyngeal swab. Subjects were included in the analyses only if their lung's samples were well preserved such that a high-quality histological assessment could be performed. We hence analysed 19 COVID-19 cases and 23 controls. Among the studied subjects, 15 had documented respiratory

conditions -*i.e.*, pneumonia, dyspnoea, respiratory distress- (10 COVID-19 and 5 controls), 15 had documented hypertension (7 COVID-19 and 8 controls), 11 suffered from type 2 diabetes (6 COVID-19 and 5 controls) and 10 from cardiovascular diseases (2 COVID-19 and 8 controls). Visceral adipose tissue was sampled from the omentum and mesentery region. Lungs were extensively sampled across central and peripheral regions of each lobe bilaterally. A median of seven tissue blocks (range five to nine) were taken from each lung. Liver samples were collected from the right and left lobe.

Samples were sliced into different pieces to be studied by light microscopy (LM) and transmission electron microscopy (TEM). A comprehensive methodological description for such methodologies has been described elsewhere (95).

Immunohistochemistry and morphometric analyses

The collected visceral (omental) adipose tissue, lung and liver autopsies were fixed overnight at 4ºC in 4% paraformaldehyde. Samples were then embedded in paraffin to be studied by LM and to perform immunohistochemistry and morphometric analyses. For each sample, 3 µm paraffin sections were obtained and used for immunohistochemical analyses. A comprehensive description of the protocol has been described elsewhere (95). To detect the presence of CD68+ macrophages in VAT samples, we used CD68 (Dako #M0814; dilution 1:200; antigen retrieval method by citrate buffer pH6) antibody. To study SARS-CoV-2 presence in VAT, we used the SARS-CoV-2 nucleocapsid (Invitrogen #MA-17404) and spike protein (Sino Biological #40150-T62) antibodies at different dilutions. The same antibodies were used to detect the virus on infected VeroE6 at dilution: 1:1000 for nucleocapsid protein and 1:100 for the spike protein. To assess antibody specificity, negative control in which primary antibody was omitted were always included in each set of reaction. Tissue sections were observed with a Nikon Eclipse E800 light microscope. For morphometric purposes, for each paraffin section, 10 digital images were acquired at 20X magnification with a Nikon DXM 1220 camera. CD68 positive macrophages widespread in VAT parenchyma and those organized to form CLS were counted in all images. For each subject the number of total macrophages and the density

of CLS/10^4 adipocytes were counted with the ImageJ morphometric program (RRID:SCR_003070). Adipocytes' area was measured in all patients by counting 100 adipocytes for each paraffin tissue section using ImageJ.

Histochemical staining

For Oil Red-O (ORO) staining samples were cryoprotected in 30% sucrose overnight, embedded in the optimal cutting temperature (OCT) compound medium, and then sliced to obtain 7 μm- thick cryosections by Leica CM1900 cryostat (Vienna, Austria). ORO staining was then performed on lungs (43) and liver (n=9) cryosections. In brief, dried cryosections were first placed in 60% isopropanol, then in filtrated Oil-Red O working solution (15 minutes at room temperature) and briefly washed again in 60% isopropanol and lastly in H_2O. Tissue slices were then counterstained with hematoxylin and cover with a coverslip using Vectashield mounting medium (Vector Laboratories). Lung and liver tissues organization and morphology were also studied by hematoxylin & eosin (H&E) staining on paraffin sections. Lung's hyaline membranes presence and characterization were performed on paraffin sections by H&E, periodic acid-Schiff and Masson trichome staining.

Transmission electron microscopy

For ultrastructural analyses, 3-mm thick VAT (n=4), lung (n=7) and liver (n=1) samples were further fixed in 2% glutaraldehyde-2% paraformaldehyde in 0.1 M phosphate buffer (pH 7.4) and post-fixed in Osmiun Tetroxide 1% then embedded in epoxy resin for TEM studies as described elsewhere (95). Cell pellets from the *in vitro* studies were similarly fixed in 2% glutaraldehyde-2% paraformaldehyde in 0.1 M phosphate buffer (pH 7.4) for one hour at room temperature and then embedded in epoxy-resin. A MT-X ultratome (RMC; Tucson) was used to obtained ultrathin sections (~70 nm). Ultrastructural characterization was performed on all samples using a CM10 Philips transmission electron microscope (Philips, Eindhoven, The Netherlands, http:// www.usa.philips.com).

Lipid droplets - In conventional TEM, lipid droplets are observed as round structures with a homogeneous content. Their electron density varies depending on the type of specimen, the type of fixative employed, and the degree of its penetration into the tissue. The use of Osmiun Tetroxide 1% during the post-fixation process provides a homogeneous, "greyish" colour to the lipid droplets, which appear to lack internal structures. Importantly, the surface of lipid droplets lacks the phospholipid bilayer typical of other organelles but displays a phospholipid monolayer. Differently from other organelles the shape of the lipid droplet is always spherical as it minimizes the interface between the hydrophobic lipid esters and the aqueous cytosol.

Statistical analysis

Between-group comparisons for linear and categorical variables were determined by unpaired two-tailed Student's t-test and Chi-square test, respectively. Group differences were considered significant when $p<0.05$. Data in graph are expressed as mean ± SEM. Statistical analyses were performed with Prism 6.0 (GraphPad Software Inc., La Jolla, CA) and IBM SPSS Statistics Data Editor (v.24).

SARS-CoV-2 infection in VeroE6

Vero E6 cells were cultured in Dulbecco's modified Eagle medium (DMEM, Euroclone, Milano, Italy), supplemented with 10% fetal calf serum (FCS Euroclone) and antibiotics/antimycotic (100 U/ml penicillin, 100 µg/ml streptomycin, 0.25 µg/ml amphotericin B) at 37°C, 5% CO_2 in a humidified atmosphere (90%), as described previously (96). Cells were maintained in 75 cm^2 tissue culture flasks. The day before infection, a confluent monolayer was trypsinized, and 1,5 x 10^6 cells were seeded in every 8 flasks (25 cm^2). Confluent monolayers were infected with SARS CoV-2 (78952 isolate, accession no. MT483867) (97) at a multiplicity of infection (MOI) of $3.29 \cdot 10^5$. After 2 hours of incubation, the medium containing the inoculum was removed, the cells were washed twice, and fresh medium was added, which was collected after 6, 12, 24 and 48 h for viral genome quantification and replaced with 2 ml of fresh culture medium to allow scraping of the infected monolayer. Uninfected cell monolayer controls were treated as infected ones. Cell suspensions (2ml)

were subsequently centrifuged at 800 rpm for 5 minutes. Aliquots of infected supernatants, collected as above, were analyzed using RT-qPCR assay as described elsewhere (97). Briefly, 5 µl of RNA extracted from 140 µl of infected supernatants were run together with a calibration curve, obtained from 10-fold dilutions of a standard plasmid certified and quantified by a supplier (2019-nCoV Positive Control, nCoVPC, 85 IDT) and negative control, applying a protocol described by CDC (https://www.fda.gov/media/134922/download).

In vitro studies on hMADS

Ethical Approval: Human adipocytes progenitors -Aps- (hMADS cells) were isolated from adipose tissue, as surgical scraps from surgical specimen of various surgeries of young donors, with the informed consent of the parents. All methods were approved and performed in accordance with the guidelines and regulations of the Centre Hospitalier Universitaire de Nice Review Board.

Cell Differentiation- hMADS cells were maintained and differentiated as previously described (98). They will be further referred to as hMADS-adipocytes. They were routinely tested for the absence of mycoplasma. Treatments and biological assays were carried out in duplicates on control or differentiated hMADS cells from day 4 to 18.

Gene expression analysis- Total RNA was extracted using the TRI-Reagent kit (Euromedex, Soufflweyersheim, France) and reverse transcription (RT) was performed using MMLV reverse transcriptase (Promega, Charbonnieres, France), as recommended by the manufacturers. All primer sequences are described in the supplementary section. Real-time PCR assays were run on an ABI Prism One step real-time PCR machine (Applied Biosystems, Courtaboeuf, France). Normalization was performed using *36B4* as a reference gene. Quantification was performed using the comparative Ct method. The results are shown as mean $\pm$ standard error of the mean (SEM), with the number of experiments indicated. Statistical significance was determined by *t*-tests BiostaTGV (INSERM and Sorbonne University, PARIS, France). Probability values <0.05 were considered statistically significant and are marked with a single asterisk, <0.01 with double asterisks and <0.001 with triple

asterisks. Sequences for the primers used in this study *ACE2* (FW 5'-AGAACCCTGGACCCTAGCAT -3'; REV 5'- AGTCGGTACTCCATCCCACA -3'); *BASIGIN* (FW: 5'-CAGAGTGAAGGCCGTGAAGT -3'; REV: 5'ACTCTGACTTGCAGACCAGC-3'); *NRP1 (FW:* 5'-GGGGCTCTCACAAGACCTTC 3'; REV: 5'- GATCCTGAATGGGTCCCGTC -3'); *CSTL* (FW: 5'-CTGGTGGTTGGCTACGGATT -3'; REV: 5'- CTCCGGTCTTTGGCCATCTT -3'); FURIN (FW:5'-CTACAGCAGTGGCAACCAGA-3'; REV:5'- TGTGAGACTCCGTGCACTTC-3'); *36B4 (FW:* 5'-CTACAACCCTGAAGAAGTGCTTG -3'; REV: 5'- CAATCTGCAGACAGACACTGG -3'); *DPP4*(SINO biologicals Inc. #HP100-649 (Eschborn, Germany)

hMADS Sars-CoV-2 infection- hMADS and hMADS adipocytes cells were infected with viral stock of SARS-CoV-2 (EPI_ISL_417491), at a 50% Tissue Culture Infectious Dose ($TCID_{50}$) of 2000 $TCID_{50}$/ml for 2 hours at a temperature of 37°C. Following incubation, the medium containing the inoculum was removed, the cells were washed twice, and the medium was supplemented with different specific compounds. Supernatants were collected at 24, 48, 72, 96 hours for viral genome quantification and medium renewal was performed at each sampling time. Uninfected cell monolayer controls were treated as the infected ones. Supernatants, collected as above, and cell pellets, collected at 96 hours post-infection, were analyzed using RT-qPCR as described in the VeroE6 cell section.

Cell Viability Assay (MTT Assay)- The effect of SARS-CoV-2 infection on cell viability of hMADS adipocytes was measured using the metabolic dye [4,5-dimethylthiazol-2-yl]-2,5-diphenyl tetrazolium (MTT) (Sigma, St. Louis, MO, USA). Briefly, hMADS cells were seeded in 96 well plates at a density of 4,500 cells/cm^2, differentiated and then infected with viral stock of SARS-CoV-2 for 2h at 37 °C. Following the incubation with the virus, cells were placed in supplemented medium. Time-course analyses of cell survival were determined at 24, 48, 72 and 96h. After the incubation period, the media were replaced with 100 µL MTT (0.5 mg/mL) dissolved in PBS and incubated for 3 h. MTT-containing medium was removed and 100 µl of dimethyl sulfoxide (DMSO) was added to dissolve formazan crystals formed by live cells. Absorbance was subsequently measured at 570 nm

using a BioTek Synergy HTX microplate reader (BioTek, Winooski, VT, USA). Results were expressed as percentages of viable cells relative to uninfected controls.

Nuclear morphology analyses- Alterations in nuclear morphology were determined by assessment of nuclear staining using fluorescent stains and fluorescent microscopy (99).

For these experiments, hMADS adipocytes were differentiated in 2-well Lab-Tek Chamber Slides (Nalge Nunc International, Naperville, IL, USA), washed with PBS pH 7.4 and fixed with 10% paraformaldehyde in PBS for 10 min at RT. After washing with PBS, nuclear staining was performed with Hoechst. Finally, cells were airdried and cover-slipped using Vectashield mounting medium (Vector Laboratories, Burlingame, CA, USA) and analyzed by fluorescent microscopy. The number of altered nuclei were counted (in the field displaying nuclear fragmentation, nuclear condensation) and divided by the total number of nuclei and multiply by 100. Observations were carried out by Lucia IMAGE 4.82, Laboratory Investigations Morphometric Analyses.

Lipid droplet size (μm^2) was measured on SARS-CoV-2 infected hMADS adipocytes and in untreated controls. For this purpose, we used a drawing tablet and a morphometric program (Nikon LUCIA IMAGE, Laboratory Imaging, version 4.61; Praha, Czech Republic). hMADS adipocytes were examined with a Nikon Eclipse Ti-S inverted light microscope (Nikon Instruments S.p.A, Calenzano, Italy), and digital images were captured at 20X with a Nikon DS-L2 camera (Nikon Instruments S.p.A, Calenzano, Italy). Five random fields were analyzed and at least 1700 lipid droplets were measured for each sample, and the difference between infected and non-infected cells was assessed by unpaired t-test. Similarly, the quantitative assessment of the material extruded from the hMADs was calculated using the same microscope and software and expressed as the number of vacuoles extruded from the cells on the total cell amount.

Results

Autoptic VAT, lung and liver samples belonging to 49 subjects were collected and screened to be included in the study. Forty-two subjects were considered suitable for the study (good-preservation for histomorphological analyses), 19 of which died due to COVID-19-related bilateral pneumonia (COVID-19 group), while the remaining 23 died for different reasons (control group). Subjects' characteristics, including gender, age, BMI, comorbidities, and cause of death are reported in supplementary table 1 and 2 (page 45 and 49, respectively). SARS-CoV-2 infection was assessed by RT-qPCR performed on nasal pharyngeal or pharyngeal swab samples. Study population mean age was 65.0±14.3 years old, BMI was 29.0±5.4 kg/m^2 with 35.7% of patients suffering from obesity (BMI≥30.0 kg/m^2), and 45.2% being overweight (BMI≥25.0 kg/m^2). Thirty-five % of the population was composed by woman (n=15). There were no significant differences in mean age (COVID-19: 69.5±11.0 vs controls: 61.0±16.0 years old; p=0.09) and BMI (COVID-19: 30.0±5.0 vs controls: 28.1±5.6 kg/m^2; p=0.62) between our study groups.

Unequivocal signs of chronic, low-grade inflammation in both COVID-19 and control subjects with a BMI≥25.0 kg/m^2 were observed in VAT samples (Fig.1A). However, although there were no between-groups differences in BMI and VAT adipocytes size (Fig.1B), higher prevalence of CD68+ macrophages (Fig.1C) and a trend for higher presence of CLS (Fig.1D) were evidenced in COVID-19 patients compared to controls, suggesting higher SARS-CoV-2-induced VAT inflammation. Other inflammatory cells were represented mainly by lymphocytes, but their number was negligible in all investigated cases.

We then assessed whether the higher VAT inflammation in COVID-19 individuals was associated with adipocytes death. Perilipin 1 (PLIN1) immunohistochemistry is a reliable method for identification and quantification of dead adipocytes (45, 49). However, in the present study, all samples displayed PLIN1 negative adipocytes, probably due to the autoptic nature of specimens. We hence performed a morphologic and ultrastructural study to assess VAT adipocytes stress and death. Electron microscopy showed signs of adipocytes death in proximity of CLS in both COVID-19 and

controls subjects with a BMI≥25 kg/m^2, a finding consistent with previous studies documenting adipocytes death in condition of visceral obesity (100). However, COVID-19 subjects VAT was rich in stressed and dead adipocytes (Fig. 1E-F) also in areas lacking CLS and seemingly normal at light microscopy. In line with the observed widespread death, cell remnants were evidenced in closed proximity of dying adipocytes, while free lipid droplets were often found in fat interstitial spaces (Fig.1F and 1G). Notably, large lipid vacuoles were also observed: *i.* inside endothelial cells belonging to capillaries adjacent to free lipid droplets (Fig.1H and Fig.1I); *ii.* extruding from endothelial cells into the capillary lumen (Fig.1I); *iii.* in the lumen of VAT capillaries (Fig.1J); *iv*. in macrophages near interstitial free lipid droplets (data not shown). In addition, several clusters of lipid-rich structures were found into the lumen of venules belonging to mesenteric fat samples (Fig.1K). In summary, the in-depth ultrastructural analyses of VAT autoptic samples belonging to COVID-19 subjects revealed the widespread presence of free lipid droplets (likely deriving from dead adipocytes) inside the capillary lumen, all features underlining a condition able to generate fat embolism syndrome (FES) (87).

We then aimed at assessing whether the observed VAT alterations were associated with SARS-CoV-2 local-tissue presence or if they were a consequence of the systemic infection. Although SARS-CoV-2 ability to infect human adipose tissue has been frequently speculated (12, 74, 78, 83), direct evidence of such phenomenon is limited in the literature (13), with only one study reporting the presence of the virus in mediastinal fat (101). While SARS-CoV-2 genomic RNA, nucleocapsid and spike proteins were not detectable in VAT samples of COVID-19 subjects, virus-like structures with morphology and size resembling those present in SARS-CoV-2 infected VeroE6 cells (Fig. 2A) were found in the cytoplasm of stressed adipocytes (Fig.2B). Furthermore, the presence of ribosome-like clusters, described in virus-infected cells (102) was evidenced in both, visceral adipocytes belonging to COVID-19 subjects (Fig. 2C and 2D) and SARS-CoV-2-infected VeroE6 (Fig. 2E).

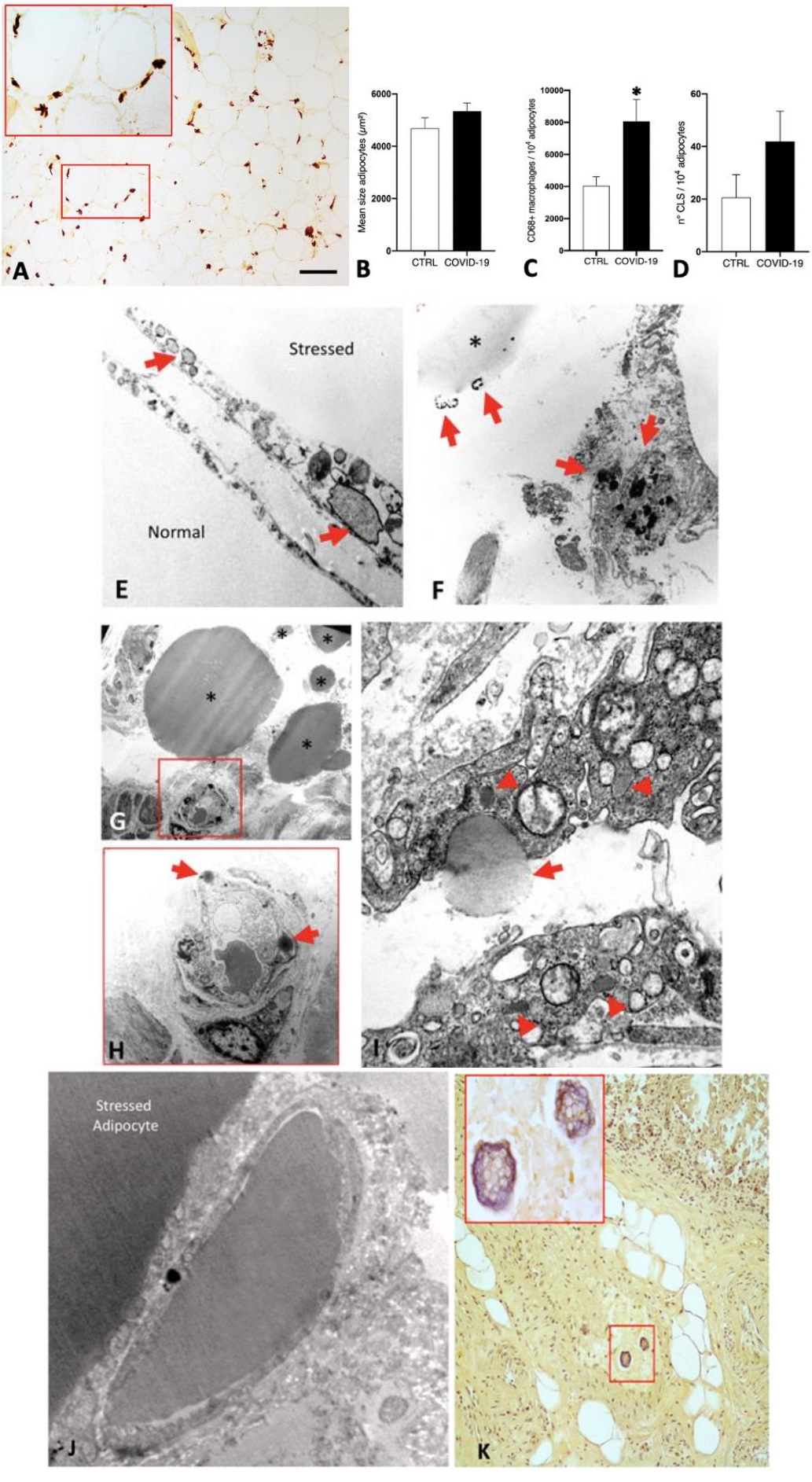
A
B
Mean size adipocytes (µm²)
6000
4000
2000
0
CTRL
COVID-19
C
CD68+ macrophages / 10⁴ adipocytes
10000
8000
6000
4000
2000
0
*
CTRL
COVID-19
D
n° CLS / 10⁴ adipocytes
60
40
20
0
CTRL
COVID-19
Stressed
Normal
E
F
G
H
I
Stressed
Adipocyte
J
K

Figure 1. Visceral adipose tissue inflammation and fat embolism in COVID-19 subjects

(**A)** Light microscopy (LM): representative immunohistochemistry of visceral adipose tissue infiltrated by CD68+ macrophages (in brown); inset shows an enlargement of the squared area. **(B)** Visceral adipose tissue adipocytes area, **(C)** number of CD68+ macrophages per 10^4 adipocytes, and **(D)** number of crown-like structures (CLS) per 10^4 adipocytes in COVID-19 vs control subjects. Asterisk (*) indicates $p<0.05$. **(E)** Transmission electron microscopy (TEM): normal adipocyte adjacent to a stressed adipocyte showing dilated endoplasmic reticulum (arrows). **(F)** TEM: dead adipocytes and interstitial free lipid droplets (*); arrows indicate adipocytes remnants. **(G)** TEM**:** free lipid droplets of variable size were frequently found in COVID-19 subjects (asterisks). **(H)** Enlargement of squared area in G showing lipid droplets inside endothelial cells (arrows). **(I)** TEM: enlargement of a capillary from a COVID-19 subject showing a lipid droplet extruding into the capillary lumen (arrow), note the abundant Weibel-Palade bodies denoting increased blood hypercoagulability (arrowheads). **(J)** TEM: a capillary filled with embolic fat near a stressed adipocyte. **(K)** LM: mesenteric fat sample showing lipid-rich embolic material in a vein (squared area, enlarged in inset). Morphometric data are expressed as means ± SE. Scale Bar: A=100 μm, E=0,8 μm, F=2,5 μm, G=10 μm, H=3 μm, I=1,5 μm, J=0,8 μm, K= 35 μm.

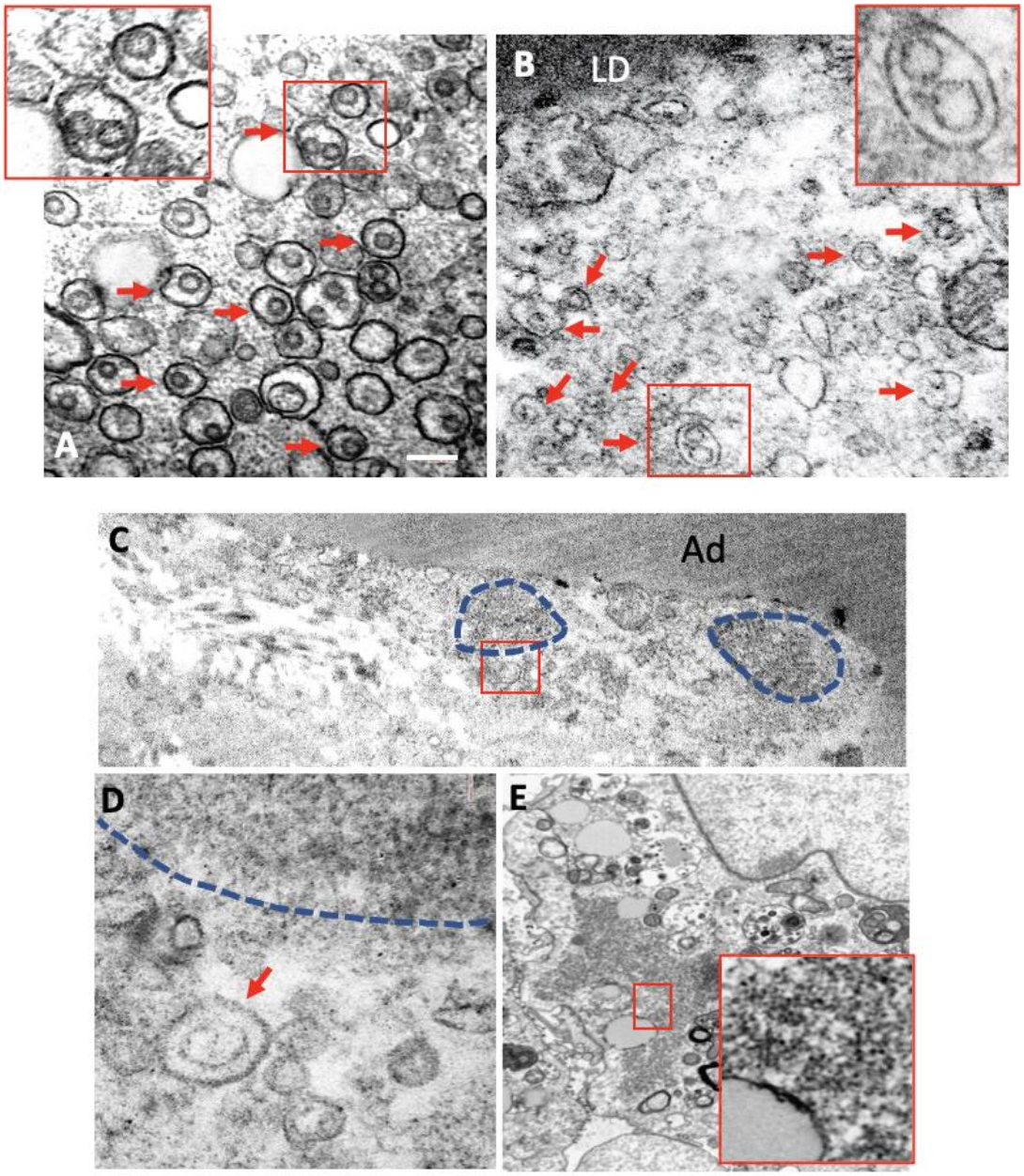

Figure 2. SARS-CoV-2 in visceral adipose tissue and hMADS

(A) Transmission electron microscopy (TEM): Vero E6 infected cell showing several virions into the rough endoplasmic reticulum (RER), some indicated by arrows. Inset: enlargement of squared area. **(B)** TEM: adipocyte from the visceral adipose tissue (VAT) depot of a COVID-19 subject showing several virions into RER (arrows). Inset: enlargement of squared area. **(C)** TEM: VAT of a COVID-19 subject showing an adipocyte (Ad) with two large ribosome-like clusters (dotted lines) in the cytoplasm. **(D)** Enlargement of squared area in C showing ribosome-like cluster and a virion-like structure into the dilated RER (arrow). **(E)** TEM: SARS-CoV-2 infected VeroE6 cell showing a ribosome-like cluster (squared area), enlarged in the inset. Scale Bar: A, B =200 nm, C=500 nm D=100 nm E=180 nm, F=120 μm, G=70 μm, H=5 μm.

In addition, confronting cisternae, ribosome lamella complex and annulate lamellae, typical of several pathologic conditions including virus infection (103), were observed in VAT adipocytes belonging to COVID-19 subjects (Fig.3 A-D) and in SARS-CoV-2 infected VeroE6 (Fig.3E), but not in uninfected controls.

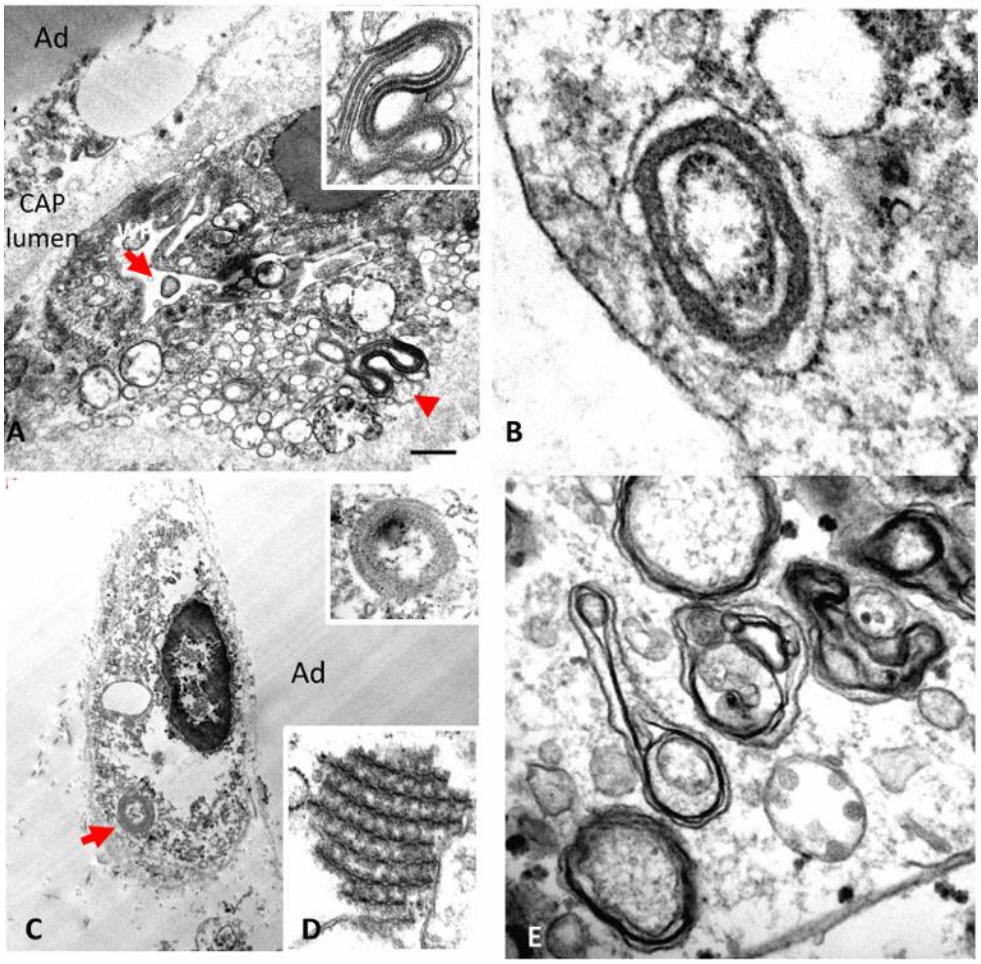

Figure 3 Representative transmission electron microscope images of visceral adipose tissue from COVID-19 subject and VeroE6 infected cells.

(A) Rough endoplasmic reticulum (RER) confronting cisternae in endothelial cell (arrowhead in A, enlarged in inset). **(B)** RER confronting cisternae in endothelial cell comparable to those found in infected VeroE6 cells (compare with E). **(C)** Ribosome-lamella complex in a capillary (arrow, enlarged in upper inset). **(D)** Annulate lamellae found in a lung's macrophage. **(E)** RER confronting cisternae in SARS-CoV-2 -infected Vero-E6 cell. Ad: adipocyte. Scale bar: A=0,8 μm, B=120 nm, C=1,2 μm, D= 200 nm, E=40 nm.

Next, to provide direct evidence of SARS-CoV-2 ability to infect human adipocytes, leading to cell stress and death, we infected differentiated human multipotent adipocytes (hMADS) (Fig. 4) and studied SARS-CoV-2 kinetics *in vitro*. The growth kinetics of SARS-CoV-2 was determined as viral load (copies/ml) in the supernatants collected after 24-, 48-, 72- and 96-hours post-infection (Fig. 4A). While SARS-CoV-2 genomic RNA was detectable in both, differentiated and undifferentiated hMADS at the first timepoints post-infection (24 and 48 h), it could be detected only in mature adipocytes at later timepoints (72 and 96 h) (Fig. 4A). Consistently, SARS-CoV-2 genomic RNA was also detected in the hMADS adipocytes pellet after 96-hours of infection (Fig. 4B). Importantly, infected hMADS adipocytes displayed lower cell viability (Fig. 4C), higher prevalence of pyknotic nuclei (Fig. 4D-E) and smaller lipid droplet size -suggestive of cell delipidation and stress- compared to uninfected controls (Fig. 4F).

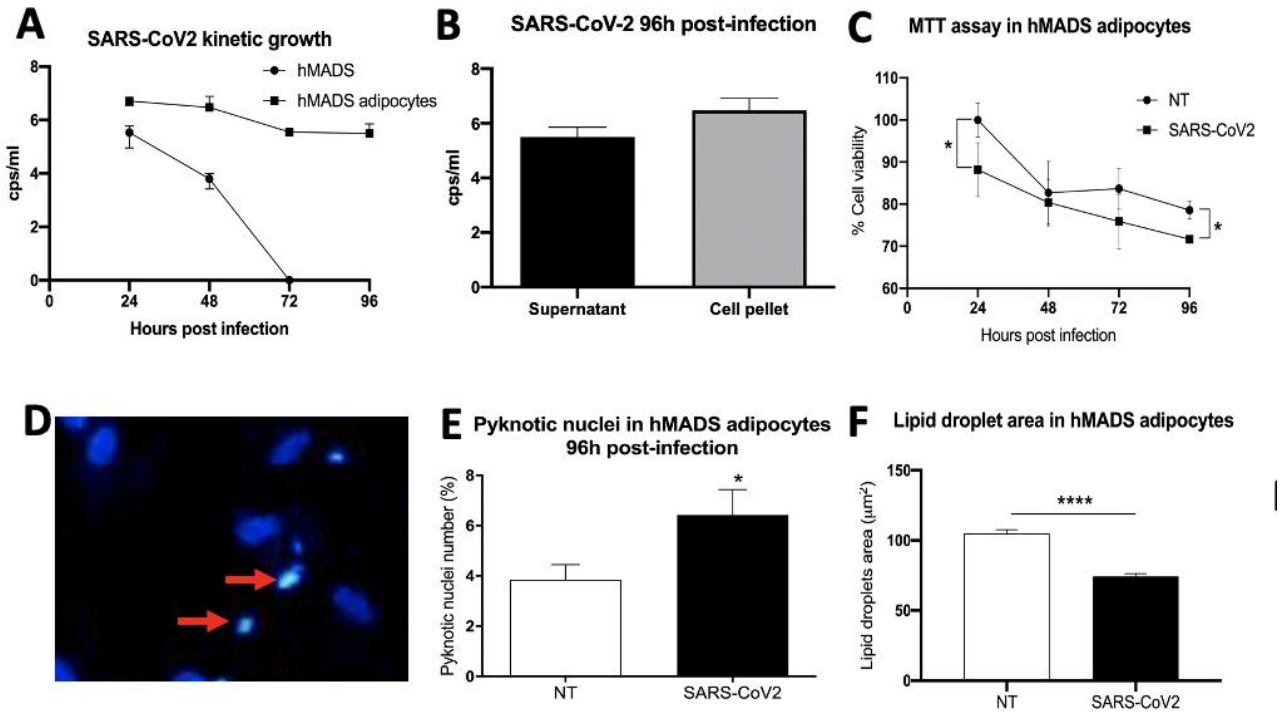

Figure 4 SARS-CoV-2 infection of hMADS (A) SARS-CoV-2 infection kinetic in undifferentiated and differentiated hMADS (hMADS adipocytes). SARS-CoV-2 genomic RNA detected in the supernatant at different timepoints, expressed as copies (cps)/ml. **(B)** SARS-CoV-2 quantification in supernatant and cell pellets of hMADS infected cells. **(C)** MTT viability assay in SARS-CoV-2 infected and non-treated (uninfected) hMADS adipocytes shows lower cell viability in the first

compared to the last at 24- and 96-hours post-infection ($p<0.05$). **(D)** Hoechst nuclear staining showing pyknotic nuclei (arrows) in differentiated hMADS adipocytes. **(E)** Percentage of pyknotic nuclei in hMADS adipocytes at 96h post-infection compared to non-treated controls ($p<0.05$). **(F)** Lipid droplets average area (μm^2) in differentiated hMADS 96h post infection compared to non-treated (uninfected) controls ($p<0.0001$).

Furthermore, in line with these data, evidence of increased material extrusion from infected cells were evidenced by light microscopy ($p<0.05$) and strongly suggested massive cell delipidation induced by SARS-CoV-2 (Fig. 5A-C). We hence performed a time-course analyses of hMADS expression of putative SARS-CoV-2 receptors and proteases (Fig. 6) in presence or absence of the adipogenic differentiation cocktail (at 4, 7, 14 and 18 days). *ACE2* receptor was expressed at very low levels in both differentiated and undifferentiated hMADS, even though we used specifically designed primers holding a 100.92% efficiency. On the other side, *BASIGIN* receptor was preferentially detected in differentiated hMADS which displayed an increased expression after 14 days. The receptor *NEUROPILIN* 1 was expressed by undifferentiated cells. Concerning proteases expression, while differentiated hMADS expressed the protease *FURIN*, the undifferentiated ones preferentially expressed *DPPIV*. The expression of *CATHEPSIN L* did not differ between the two conditions, while we did not detect *TMPRSS2* in both differentiated and undifferentiated hMADS (data not shown).

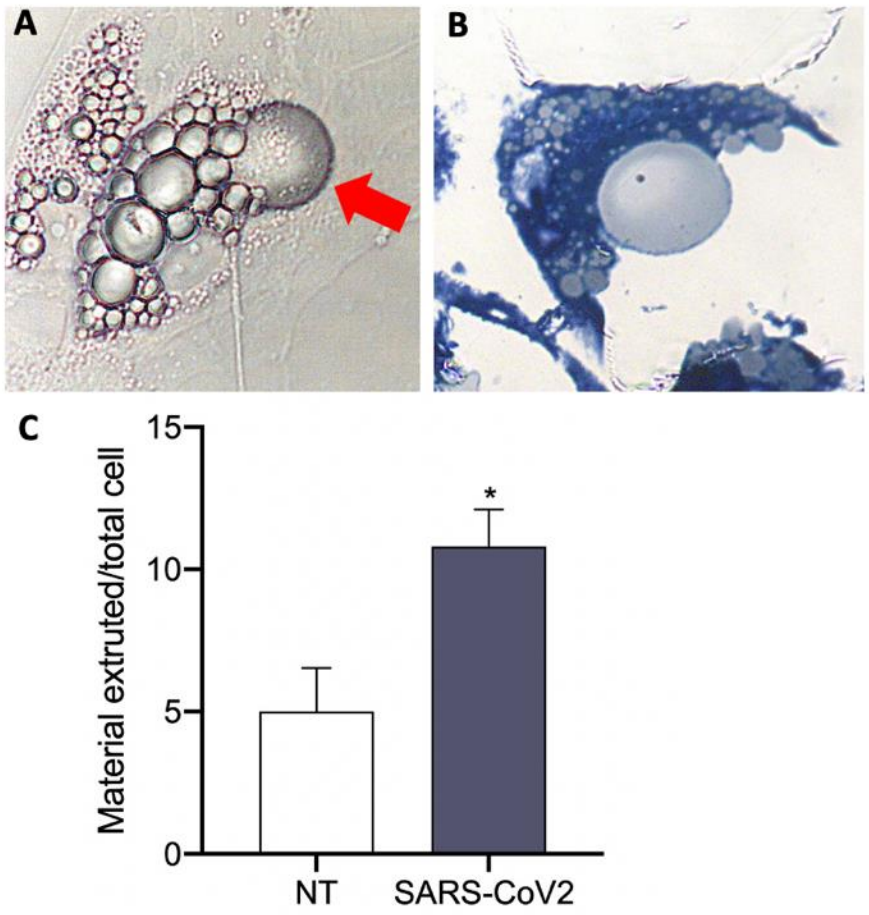

Figure 5. hMADS delipidation following SARS-CoV-2 infection. **(A)** Light microscopy of differentiated human adipocytes (hMADS) extruding lipid-like material. **(B)** Toluidine staining of an hMADS cell extruding a lipid vacuole (resin-embedded). **(C)** Quantitative analyses of the amount of material extruded from the cell in SARS-CoV-2 infected and non-treated (uninfected) hMADS.

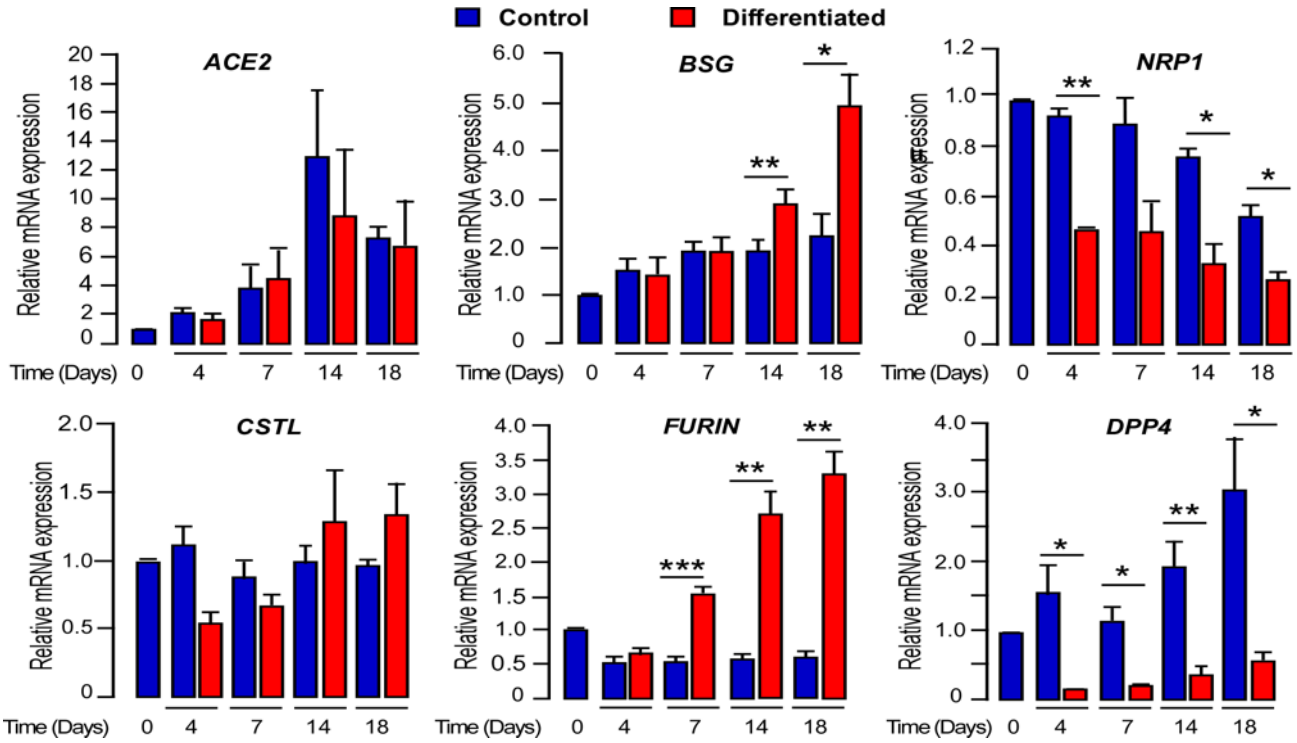

Figure 6. Expression of SARS-CoV-2 receptor and proteases in differentiated hMADS and undifferentiated (controls). Expression of putative SARS-CoV-2 receptors or proteases assessed by RT-qPCR and normalized for the expression of *36B4* mRNA. Expressions were measured in cells that received (red bars-differentiated-) or did not receive (blue bars-controls-) the differentiation cocktail for the indicated number of days. The means ± SE were calculated from three independent experiments (*ACE2, BSG, NRP1, CSTL*) or four independent experiments (*FURIN, DPP4*), with determinations performed in duplicate (*p<0.05, ** p<0.01).

Given our preliminary data (83) and the widespread lipid droplets presence in the capillary lumen of VAT, also evidenced in some mesenteric adipose depots, we then studied lipid distribution in lung samples employing Oil-Red O staining (ORO: lipid-specific histochemistry). Lipids were evidenced within lungs alveolar septa, interstitial spaces, endothelial cells, and vessel's lumen and in alveolar and interstitial macrophages (Fig. 7A-D), all features confirmed by light and electron microscopy (Fig. 7E-F) and suggestive of fat embolism (21).

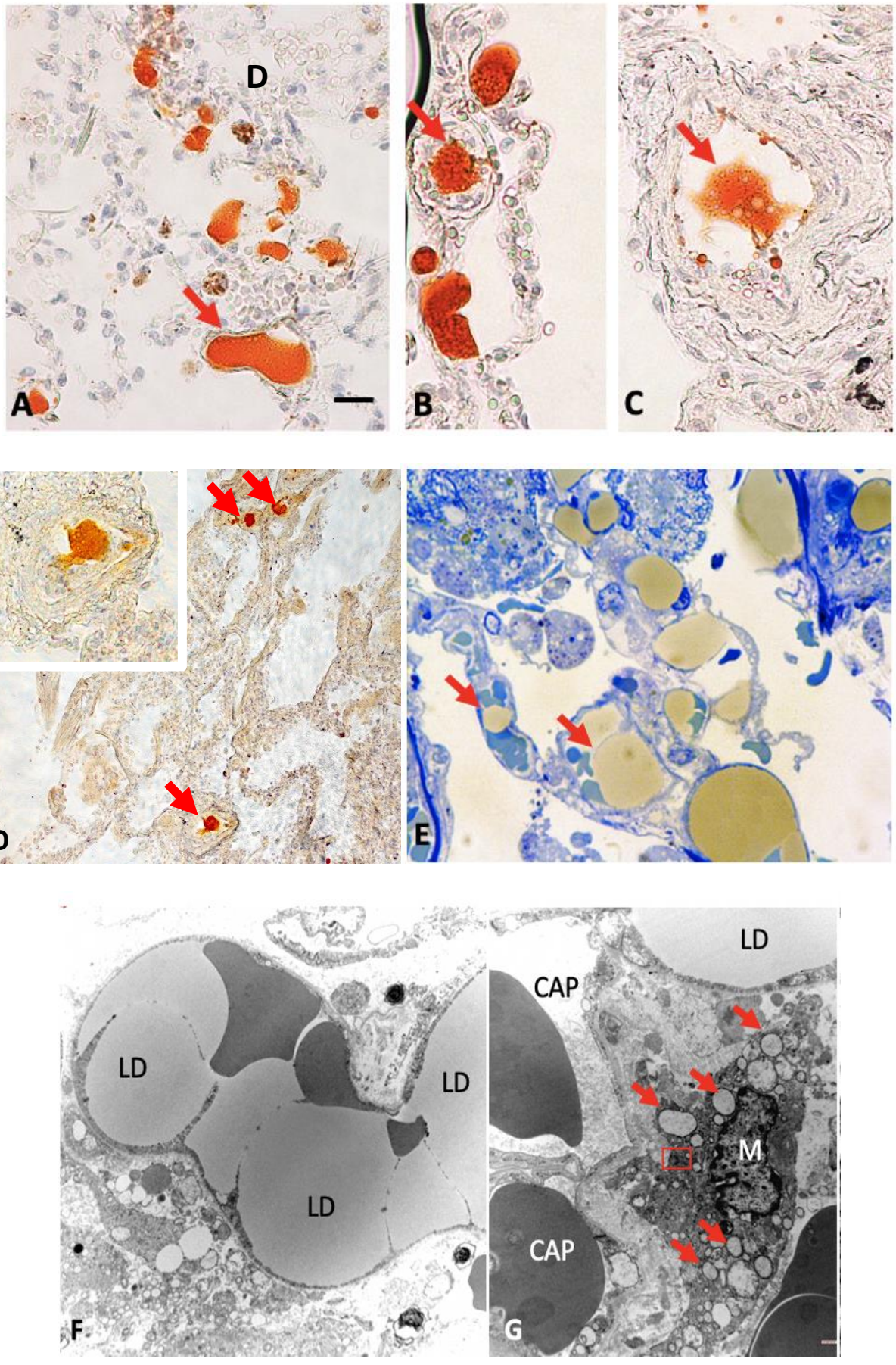
A
B
C
D
D
E
F
G
LD
LD
LD
LD
CAP
CAP
M

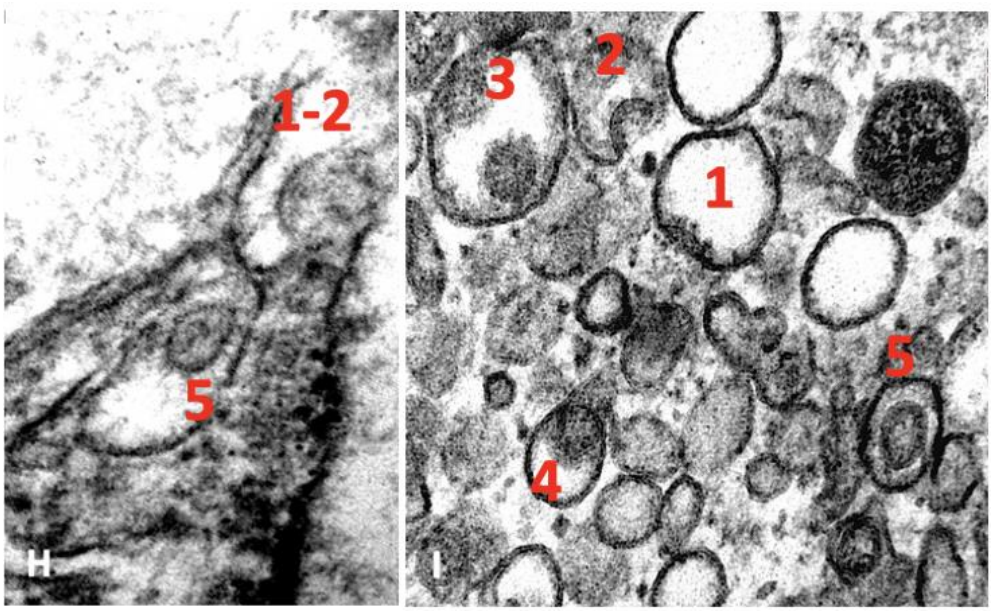

Figure 7. Embolic lipid droplets and SARS-CoV-2 virions in lung of COVID-19 subjects.
(A-D) Light microscopy (LM): representative histochemistry for fat (Oil-Red O) showing the lipid nature of vacuoles (orange-red) in the vascular lumen (arrows) and lung septa of different COVID-19 subjects. **(E)** LM: resin embedded, toluidine-blue stained tissue. Large free lipid droplets (yellow) are evident into the capillaries lumen in alveolar septa (arrows). **(F)** Transmission electron microscopy (TEM): showing lipid droplet (LD) into an alveolar septum mixed with erythrocytes. **(G)** TEM: alveolar macrophage (M) in a COVID-19 subject. Note: diffuse dilated rough endoplasmic reticulum (RER) denoting cellular stress (arrows). **(H)** TEM: enlargement of the squared area in G showing two virions at stages 1-2 and 5 of the reproductive cycle into the dilated RER similar to what observed in **(I)** TEM: (1 to 5) stages of reproductive cycle of SARS-CoV-2 virions in VeroE6 infected cells. Reference in the main text. Scale Bar: A, B, C=20 μm, D=140 μm E=8 μm, F=1,5 μm, G=1 μm, H=70 nm I=65 nm.

Lung's fat embolism was not exclusive of, but more prevalent among COVID-19 subjects as compared to controls (100% vs 53%; $p<0.001$). Signs of fat embolism were in fact more prevalent among individuals with obesity than in those with a BMI≤30 kg/m^2 (93% vs 63%, $p=0.03$), independently of COVID-19 diagnosis. Consistently, all subjects with T2DM had fat embolism. Of note, electron microscopy observation revealed several structures with size and morphology compatible with those of SARS-CoV-2 viruses (4) in pneumocytes, endothelial cells and macrophages, the last of which displayed disseminated, dilated endoplasmic reticulum denoting

cellular stress (46, 100) and signs of virus presence only in COVID-19 subjects. Furthermore, we also evidenced also two virions at early and late stages of reproductive cycle (104) into the dilated endoplasmic reticulum (Fig. 7H) comparable with those revealed in infected VeroE6 in Fig. 7I. Nascent particles are formed through the juxtaposition of the viral nucleocapsid along the cytoplasmic membrane proximal to the budding compartment (between RER and Golgi complex) or along RER (102). Therefore, virions acquire an envelope by budding in the cisternae. They then form a spherical/pleomorphic particle of ~80 nm in diameter (102). Importantly, septal capillaries very often contained large amounts of fibrin, with some of them lining by fibrin-thrombotic material only in COVID-19 individuals' lungs (data not shown). Several Weibel-Palade bodies, signs of activated coagulative phenomena (103), were observed also in capillary endothelial cells belonging to COVID-19 subjects (data not shown).

Unexpectedly, the ORO technique evidenced also positively stained alveolar structures reminiscent of hyaline membranes (Fig. 8A). The presence of hyaline membranes was then confirmed by hematoxylin and eosin, by Mallory and periodic acid-Schiff staining (data not shown). All COVID-19 subjects presented lung's hyaline membranes, which were on the other side detected only in one control subject (BMI= 21.3 kg/m^2) who died due to pneumonia ($p<0.0001$). Interestingly, this last subject displayed fainted lung's hyaline membrane positivity for ORO staining, suggesting a lower lipidic composition. This finding is consistent with other reports describing hyaline membrane presence in pneumonia (11). Importantly, ORO positive lipid droplets and lipid-rich macrophages were often enclosed into the hyaline membranes lining the alveolar surface (Fig. 8B-D). Several aspects suggesting a direct role of embolic fat in hyaline membranes formation were observed. Specifically, free lipid droplets occupying the alveolar space and lining and spreading on the alveolar surface were observed (Fig. 8E-H).

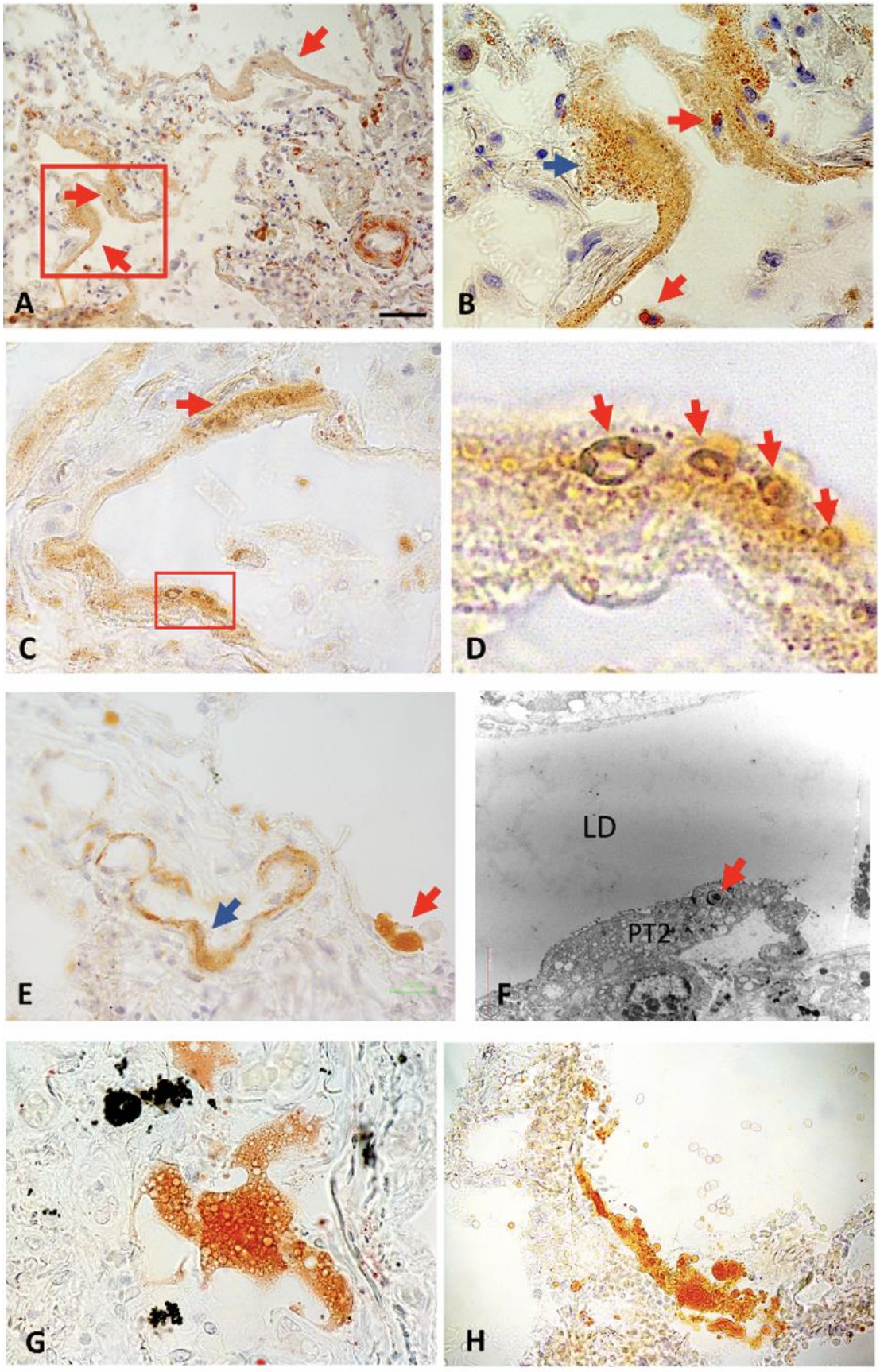
A
B
C
D
E
LD
PT2
F
G
H

Figure 8. Oil-Red O-stained lung of COVID-19 subjects showing hyaline membranes morphology and composition

(A) Light microscopy (LM): hyaline membranes lining alveolar surfaces (arrows) at low magnification. **(B)** LM: enlargement of squared area in A showing the microvacuolar nature of ORO+ hyaline membranes (blue arrow). Lipid rich macrophages free in the alveolar space (red arrows) and inside hyaline membranes (blue arrows). **(C)** LM: vacuolar aspect of ORO+ hyaline membranes' lipids (arrow and squared area). **(D)** LM: enlargement of squared area in C. Arrows indicate lipid vacuoles. **(E)** LM: ORO+ large, free lipid vacuole lining the alveolar surface (red arrow) near a hyaline membrane (blue arrow). **(F)** Free lipid droplet lining the alveolar surface composed by pneumocytes type II (PT2) with classic surfactant granules (arrow) by transmission electron microscopy. **(G)** LM: ORO+ lipid vacuole spreading on the alveolar surface (possible early stage of lipid diffusion). **(H)** LM: ORO+ lipid vacuoles possibly contributing to hyaline membranes development (later stage). Scale Bar: A and E= 50 µm, B=7 µm, C=10 µm, D=2 µm, F=3 µm, G=25 µm, H=35 µm.

The presence of lung's hyaline membranes of lipidic nature was associated with visceral adipose tissue inflammation (8.0±5.4 vs 3.7±1.8 CD68+ macrophages/10 adipocytes in subjects with and without hyaline membranes, respectively) and exclusive of COVID-19 cases (Fig. 9).

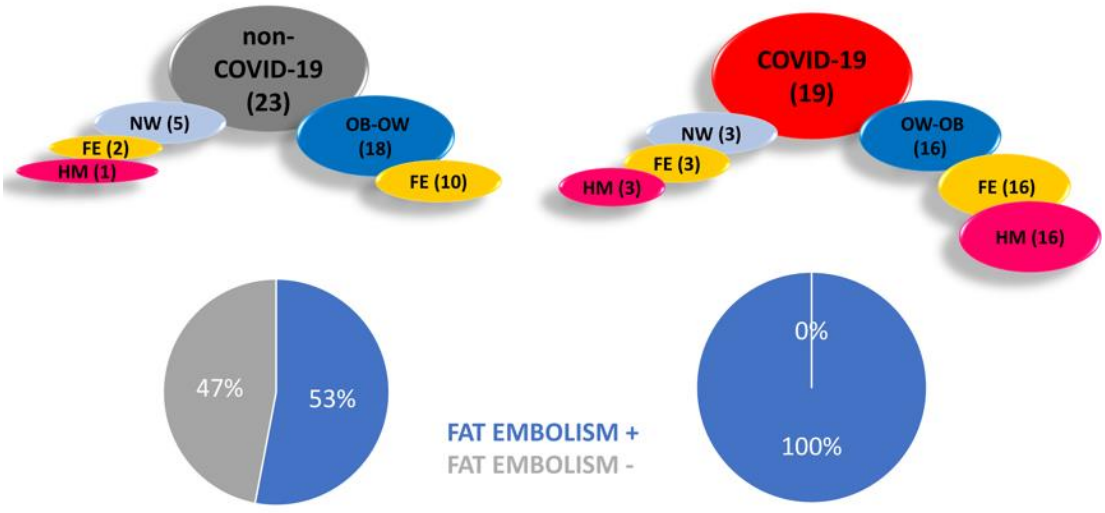

Fig. 9 Schematic representation of the prevalence of fat embolism (FE) and lipidic hyaline membranes (HM) in the study population. Weight status *i.e.*, OW-OB: overweight and obese subjects with BMI: body mass index (kg/m^2) ≥25); NW: normo-weight subjects with BMI<25 kg/m^2. Number of patients for each category is reported in parenthesis. Prevalence (%) of fat embolism among subjects with and without COVID-19 are reported in the pie chart.

Lastly, since the embolic material from abdominal visceral tissues should necessarily pass through the liver parenchyma to reach the lung, we exploited the ORO staining technique to study liver samples belonging to 9 COVID-19 and 8 control subjects. Liver autoptic samples showed focal, macrovescicular steatosis with lipid droplets of very variable size (Fig. 10A), consistent with other studies conducted on COVID-19 subjects (105). Signs consistent with fat embolism, *i.e.*, presence of free lipid droplets into hepatic sinusoids (Fig. 10B) and into the vessels' lumen (Fig. 10C-D), as well as clusters of lipid-rich structures in the portal vein (Fig. 10D) were observed in COVID-19 subjects, a finding that confirmed the embolic nature of hepatic fat droplets, and that support what observed in VAT samples. In summary, 8/9 COVID-19 subjects with documented lung fat embolism displayed signs of hepatic fat embolism as well. On the other side, we observed hepatic embolism in an elevated percentage of control subjects (6/8), possibly due to the elevated prevalence of visceral obesity among these investigated cases.

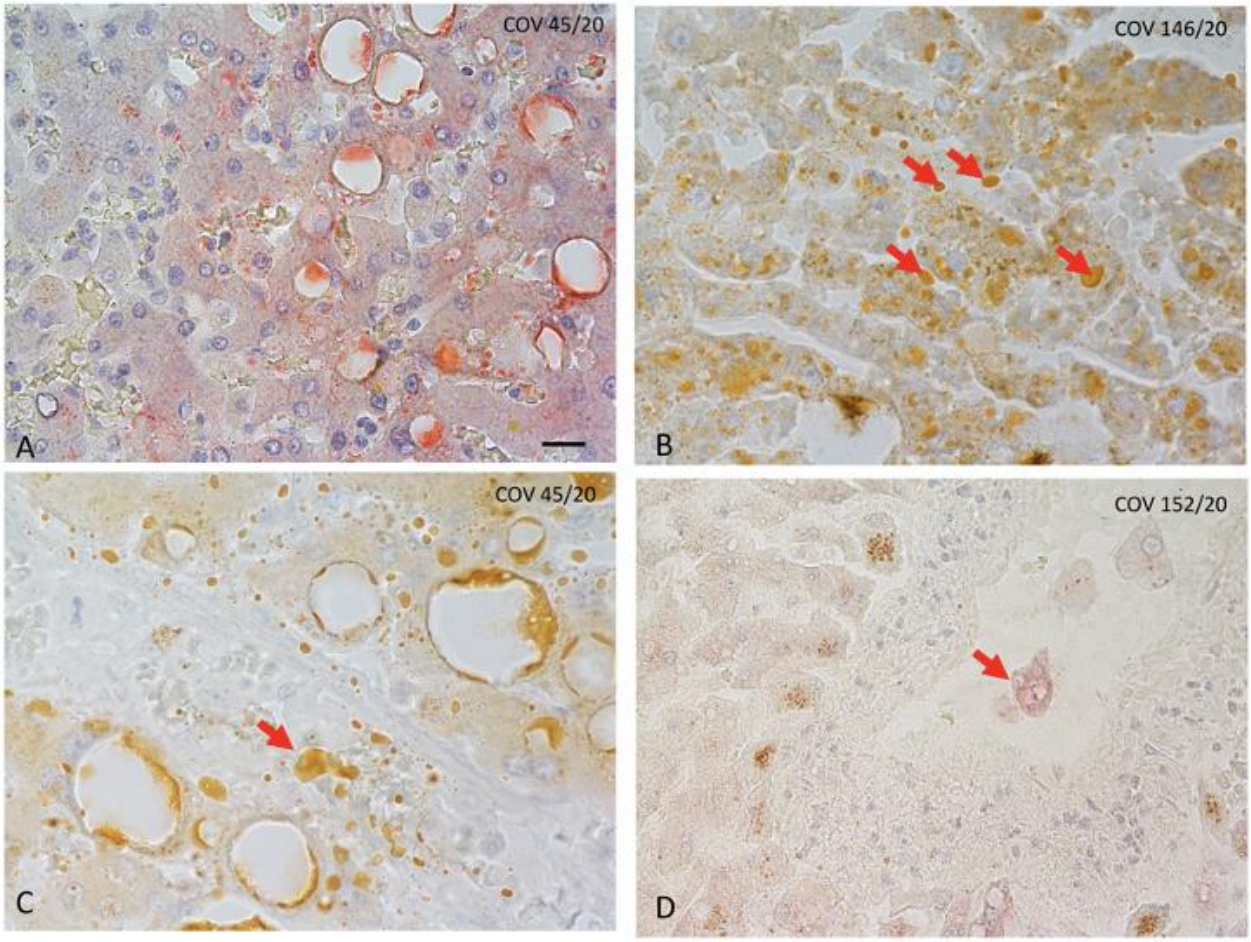

Figure. 10 Fat embolic features in liver of three different COVID-19 subjects with documented lung fat embolism. (A) Focal, macrovescicular steatosis evidenced by Oil-Red O staining (ORO). **(B)** Several ORO+ lipid droplets into sinusoids (arrows). **(C)** Portal area enlargement of subject shown in B. Note the large lipid droplets into the portal vein lumen (arrow). **(D)** Cluster of lipid rich vacuoles (arrow), like the one found in the mesenteric adipose tissue vein shown in Fig.1K. Scale bar: A=10 mm, B=7 mm, C=8mm, D=13 mm.

Discussion

This is the first study investigating the ultrastructural features of VAT among COVID-19 subjects and assessing lipids distribution in lungs and liver samples by histomorphology. Our data support the presence of higher local VAT inflammation and higher prevalence of fat embolism and lipidic hyaline membranes formations in the lungs of subjects dead due to COVID-19 compared to control individuals' dead for different reasons. In addition, our data support SARS-CoV-2 ability to infect human adipocytes *in vitro*. Considering the strong association between COVID-19 related complications and obesity, most especially visceral obesity (13, 72-76), the comprehension of the biological phenomenon at the basis of such association holds critical clinical implication in the era of the COVID-19 pandemic.

Our study provides the first evidence of higher local VAT inflammation among COVID-19 subjects, independently of obesity status and support COVID-19-induced exacerbation of obesity-related inflammation, a novel finding consistent with studies reporting higher systemic inflammation among infected patients (78). Adipocyte's inflammation is associated with adipocytes stress, death, and lipids release in the extracellular space (45, 49, 85, 100). We hence studied adipocytes features by TEM and revealed the presence of the typical signs of cellular stress, together with clear features of lipids' spill-over from suffering adipocytes. Lipids were in fact detected in the extracellular space, inside endothelial cells, inside the capillary lumen, and extruding from endothelial cells into the capillary lumen, all features indicative of fat embolism.

Although virus like structures were evidenced by TEM in the same VAT depots, the lack of SARS-CoV-2 detection by qPCR did not allow us to conclude that such inflammation, cellular stress, and death were all related to the direct presence of this virus. It is in fact possible that the described VAT features were secondary to the systemic inflammation induced by COVID-19 or due to the presence of different viruses within the depot (superinfection). On the other side, we were able to demonstrate that SARS-CoV-2 can infect human adipocytes even though neither adipocytes, nor adipocytes progenitors gathered all the known molecular requirements for the virus entry (expression

of all known virus proteases and receptors). This set of data is in part consistent with other findings and suggest that additional, not yet characterized, receptors and proteases may be exploited for this purpose (13, 106).

Considering the widespread lipid droplets presence in the capillary lumen of VAT and considering our preliminary data (83), we studied lipid distribution in lung and liver samples and confirmed the presence of fat embolism. Interestingly, we noticed similar lipid-like structures also in lung's images from other reports on COVID-19 subjects, reason for which we believe it is worth performing further in-depth analyses on available samples (3, 4, 107).

Fat embolism was more prevalent among, but not exclusive of, subjects with COVID-19; it was in fact detected also, and was more prevalent, among subjects with obesity independently of SARS-CoV-2 infection. Importantly, 100% of T2DM subjects enrolled in the study presented fat emboli. These data are not surprising given that adipocyte's death and release of lipids are both phenomena occurring in obesity and associated with obesity-related metabolic complications including T2DM (45, 49, 100). This finding provides the first evidence pointing towards fat embolism as a complication of obesity (and obesity plus T2DM), determined by adipocytes death and possibly exacerbated by the COVID-19-induced inflammatory status. Importantly, studying lung's lipid distribution, we unexpectedly revealed the presence of lipidic hyaline membranes, formation strongly contributing to and associated with COVID-19 related interstitial fibrosis, pneumonia and acute respiratory syndrome disease (4). Hyaline membranes formations are a histological hallmark of the diffuse alveolar damage and are considered responsible for the impairment in lungs oxygen exchange, hence respiratory failure (11). Hyaline membranes are visible as dense, eosinophilic amorphous material, distributed along alveolar septa and are documented to be composed by cellular debris, plasma protein (*i.e.*, albumin, fibrinogen, and immunoglobulin) and surfactant components (108, 109). However, the steps involved in their etiology have not been characterized. In our study we revealed for the first time the lipidic nature of hyaline membranes which were present in all COVID-19 subjects and in only one control individual who died due to pneumonia. This finding is consistent

with other reports describing hyaline membrane presence in pneumonia (11). Our histomorpholgic assessment revealed several aspects indicative of a direct role of embolic fat in hyaline membranes formation. Consistently, the presence of lung's hyaline membranes of lipidic nature was associated with visceral adipose tissue inflammation, which was in fact higher among COVID-19 cases.

In summary, in our case series, although fat embolism may be present in condition of obesity and T2DM independently of COVID-19, the embolic-derived lipidic material contribute to the formation of hyaline membranes only in the case of COVID-19 related pneumonia, a novel finding that holds critical clinical implications and deserves further investigation. Furthermore, these data provide significant insight into hyaline membrane nature, as their formation process has not been characterized yet (110). Additional studies investigating the hyaline membranes nature of non-COVID-19-related pneumonia are required to detail such histopathological feature.

Collectively our data reveal higher local VAT inflammation in COVID-19 subjects and SARS-CoV-2 ability to infect human adipocytes, both elements widely speculated in the literature (13, 84). In addition, we provide the first evidence that supports fat embolism as a complication of obesity, in particular metabolic unhealthy obesity, likely determined by adipocytes death and exacerbated by the COVID-19-induced inflammatory status. Lastly, we reveal for the first time the presence of lung's lipidic hyaline membranes among all infected subjects, a novel COVID-19-related histopathological feature associated with visceral adipose tissue inflammation and fat embolism. As fat embolism displays similar signs and symptoms as the ones observed in COVID-19 (93), differential diagnosis, when fat embolism and COVID-19 are suspected, is critical for proper patients' care. Based on our findings, the assessment of fat embolism symptoms is mandatory in the context of the COVID-19 pandemic, especially among patients with pulmonary symptoms, obesity and high waist circumference, signs of elevated visceral adipose accumulation. Such complex clinical status should be therefore adequately assessed and properly addressed. Our data hold critical clinical implication in the context of obesity research and the COVID-19 pandemic and need to be further investigated by additional studies with a larger sample size.

References

1. Zhu N, Zhang D, Wang W, Li X, Yang B, Song J, et al. A Novel Coronavirus from Patients with Pneumonia in China, 2019. *N Engl J Med.* 2020;382(8):727-33.
2. Medicine JHU. Coronavirus Resource Center. https://coronavirus.jhu.edu/map.html. Accessed 27th July 2021, 2021.
3. Xu Z, Shi L, Wang Y, Zhang J, Huang L, Zhang C, et al. Pathological findings of COVID-19 associated with acute respiratory distress syndrome. *Lancet Respir Med.* 2020;8(4):420-2.
4. Bradley BT, Maioli H, Johnston R, Chaudhry I, Fink SL, Xu H, et al. Histopathology and ultrastructural findings of fatal COVID-19 infections in Washington State: a case series. *Lancet.* 2020;396(10247):320-32.
5. Zhou F, Yu T, Du R, Fan G, Liu Y, Liu Z, et al. Clinical course and risk factors for mortality of adult inpatients with COVID-19 in Wuhan, China: a retrospective cohort study. *Lancet.* 2020;395(10229):1054-62.
6. Wu Z, and McGoogan JM. Characteristics of and Important Lessons From the Coronavirus Disease 2019 (COVID-19) Outbreak in China: Summary of a Report of 72314 Cases From the Chinese Center for Disease Control and Prevention. *JAMA.* 2020;323(13):1239-42.
7. Savla SR, Prabhavalkar KS, and Bhatt LK. Cytokine storm associated coagulation complications in COVID-19 patients: Pathogenesis and Management. *Expert Rev Anti Infect Ther.* 2021;19(11):1397-413.
8. Mahendra M, Nuchin A, Kumar R, Shreedhar S, and Mahesh PA. Predictors of mortality in patients with severe COVID-19 pneumonia - a retrospective study. *Adv Respir Med.* 2021;89(2):135-44.
9. Huang C, Wang Y, Li X, Ren L, Zhao J, Hu Y, et al. Clinical features of patients infected with 2019 novel coronavirus in Wuhan, China. *Lancet.* 2020;395(10223):497-506.
10. Wadman M, Couzin-Frankel J, Kaiser J, and Matacic C. A rampage through the body. *Science.* 2020;368(6489):356-60.
11. Schneider JL, Rowe JH, Garcia-de-Alba C, Kim CF, Sharpe AH, and Haigis MC. The aging lung: Physiology, disease, and immunity. *Cell.* 2021;184(8):1990-2019.
12. Stefan N, Birkenfeld AL, and Schulze MB. Global pandemics interconnected - obesity, impaired metabolic health and COVID-19. *Nat Rev Endocrinol.* 2021;17(3):135-49.
13. Drucker DJ. Diabetes, obesity, metabolism, and SARS-CoV-2 infection: the end of the beginning. *Cell Metab.* 2021;33(3):479-98.
14. Colleluori G, and Villareal DT. Aging, obesity, sarcopenia and the effect of diet and exercise intervention. *Exp Gerontol.* 2021;155:111561.
15. Bluher M. Obesity: global epidemiology and pathogenesis. *Nat Rev Endocrinol.* 2019;15(5):288-98.
16. Ward ZJ, Bleich SN, Cradock AL, Barrett JL, Giles CM, Flax C, et al. Projected U.S. State-Level Prevalence of Adult Obesity and Severe Obesity. *N Engl J Med.* 2019;381(25):2440-50.
17. RisC. ADULT BODY-MASS INDEX. https://www.ncdrisc.org/data-visualisations-adiposity.html. Accessed March 2021.
18. EASO. In: Obesity EAftSo ed.; 2020.
19. WHO. WHO European Childhood Obesity Surveillance Initiative (COSI). https://www.euro.who.int/en/health-topics/disease-prevention/nutrition/activities/who-european-childhood-obesity-surveillance-initiative-cosi.
20. Geserick M, Vogel M, Gausche R, Lipek T, Spielau U, Keller E, et al. Acceleration of BMI in Early Childhood and Risk of Sustained Obesity. *N Engl J Med.* 2018;379(14):1303-12.
21. WHO. Obesity Report. Accessed January 25th 2020.

22. Bray GA, Kim KK, Wilding JPH, and World Obesity F. Obesity: a chronic relapsing progressive disease process. A position statement of the World Obesity Federation. *Obes Rev.* 2017;18(7):715-23.
23. Batsis JA, and Villareal DT. Sarcopenic obesity in older adults: aetiology, epidemiology and treatment strategies. *Nat Rev Endocrinol.* 2018;14(9):513-37.
24. Cinti S. Adipose Organ Development and Remodeling. *Compr Physiol.* 2018;8(4):1357-431.
25. Cinti S. The adipose organ at a glance. *Dis Model Mech.* 2012;5(5):588-94.
26. Kim SM, Lun M, Wang M, Senyo SE, Guillermier C, Patwari P, et al. Loss of white adipose hyperplastic potential is associated with enhanced susceptibility to insulin resistance. *Cell Metab.* 2014;20(6):1049-58.
27. Spalding KL, Arner E, Westermark PO, Bernard S, Buchholz BA, Bergmann O, et al. Dynamics of fat cell turnover in humans. *Nature.* 2008;453(7196):783-7.
28. Muller S, Kulenkampff E, and Wolfrum C. Adipose Tissue Stem Cells. *Handb Exp Pharmacol.* 2016;233:251-63.
29. Salans LB, Horton ES, and Sims EA. Experimental obesity in man: cellular character of the adipose tissue. *J Clin Invest.* 1971;50(5):1005-11.
30. Wang QA, Tao C, Gupta RK, and Scherer PE. Tracking adipogenesis during white adipose tissue development, expansion and regeneration. *Nat Med.* 2013;19(10):1338-44.
31. Despres JP, and Lemieux I. Abdominal obesity and metabolic syndrome. *Nature.* 2006;444(7121):881-7.
32. Tchkonia T, Thomou T, Zhu Y, Karagiannides I, Pothoulakis C, Jensen MD, et al. Mechanisms and metabolic implications of regional differences among fat depots. *Cell Metab.* 2013;17(5):644-56.
33. Siervo M, Lara J, Celis-Morales C, Vacca M, Oggioni C, Battezzati A, et al. Age-related changes in basal substrate oxidation and visceral adiposity and their association with metabolic syndrome. *Eur J Nutr.* 2016;55(4):1755-67.
34. Brinkley TE, Hsu FC, Beavers KM, Church TS, Goodpaster BH, Stafford RS, et al. Total and abdominal adiposity are associated with inflammation in older adults using a factor analysis approach. *J Gerontol A Biol Sci Med Sci.* 2012;67(10):1099-106.
35. Goodpaster BH, Thaete FL, and Kelley DE. Thigh adipose tissue distribution is associated with insulin resistance in obesity and in type 2 diabetes mellitus. *Am J Clin Nutr.* 2000;71(4):885-92.
36. Cerhan JR, Moore SC, Jacobs EJ, Kitahara CM, Rosenberg PS, Adami HO, et al. A pooled analysis of waist circumference and mortality in 650,000 adults. *Mayo Clin Proc.* 2014;89(3):335-45.
37. de Hollander EL, Bemelmans WJ, Boshuizen HC, Friedrich N, Wallaschofski H, Guallar-Castillon P, et al. The association between waist circumference and risk of mortality considering body mass index in 65- to 74-year-olds: a meta-analysis of 29 cohorts involving more than 58 000 elderly persons. *Int J Epidemiol.* 2012;41(3):805-17.
38. Santanasto AJ, Goodpaster BH, Kritchevsky SB, Miljkovic I, Satterfield S, Schwartz AV, et al. Body Composition Remodeling and Mortality: The Health Aging and Body Composition Study. *J Gerontol A Biol Sci Med Sci.* 2017;72(4):513-9.
39. Ross R, Neeland IJ, Yamashita S, Shai I, Seidell J, Magni P, et al. Waist circumference as a vital sign in clinical practice: a Consensus Statement from the IAS and ICCR Working Group on Visceral Obesity. *Nat Rev Endocrinol.* 2020.
40. Weyer C, Foley JE, Bogardus C, Tataranni PA, and Pratley RE. Enlarged subcutaneous abdominal adipocyte size, but not obesity itself, predicts type II diabetes independent of insulin resistance. *Diabetologia.* 2000;43(12):1498-506.
41. Arner E, Westermark PO, Spalding KL, Britton T, Ryden M, Frisen J, et al. Adipocyte turnover: relevance to human adipose tissue morphology. *Diabetes.* 2010;59(1):105-9.

42. Guo W, Pirtskhalava T, Tchkonia T, Xie W, Thomou T, Han J, et al. Aging results in paradoxical susceptibility of fat cell progenitors to lipotoxicity. *Am J Physiol Endocrinol Metab.* 2007;292(4):E1041-51.
43. Sepe A, Tchkonia T, Thomou T, Zamboni M, and Kirkland JL. Aging and regional differences in fat cell progenitors - a mini-review. *Gerontology.* 2011;57(1):66-75.
44. Belligoli A, Compagnin C, Sanna M, Favaretto F, Fabris R, Busetto L, et al. Characterization of subcutaneous and omental adipose tissue in patients with obesity and with different degrees of glucose impairment. *Sci Rep.* 2019;9(1):11333.
45. Cinti S, Mitchell G, Barbatelli G, Murano I, Ceresi E, Faloia E, et al. Adipocyte death defines macrophage localization and function in adipose tissue of obese mice and humans. *J Lipid Res.* 2005;46(11):2347-55.
46. Giordano A, Murano I, Mondini E, Perugini J, Smorlesi A, Severi I, et al. Obese adipocytes show ultrastructural features of stressed cells and die of pyroptosis. *J Lipid Res.* 2013;54(9):2423-36.
47. Lumeng CN, Liu J, Geletka L, Delaney C, Delproposto J, Desai A, et al. Aging is associated with an increase in T cells and inflammatory macrophages in visceral adipose tissue. *J Immunol.* 2011;187(12):6208-16.
48. Cotillard A, Poitou C, Torcivia A, Bouillot JL, Dietrich A, Kloting N, et al. Adipocyte size threshold matters: link with risk of type 2 diabetes and improved insulin resistance after gastric bypass. *J Clin Endocrinol Metab.* 2014;99(8):E1466-70.
49. Murano I, Barbatelli G, Parisani V, Latini C, Muzzonigro G, Castellucci M, et al. Dead adipocytes, detected as crown-like structures, are prevalent in visceral fat depots of genetically obese mice. *J Lipid Res.* 2008;49(7):1562-8.
50. Le KA, Mahurkar S, Alderete TL, Hasson RE, Adam TC, Kim JS, et al. Subcutaneous adipose tissue macrophage infiltration is associated with hepatic and visceral fat deposition, hyperinsulinemia, and stimulation of NF-kappaB stress pathway. *Diabetes.* 2011;60(11):2802-9.
51. Wu H, and Ballantyne CM. Skeletal muscle inflammation and insulin resistance in obesity. *J Clin Invest.* 2017;127(1):43-54.
52. Lee JS, Kim SH, Jun DW, Han JH, Jang EC, Park JY, et al. Clinical implications of fatty pancreas: correlations between fatty pancreas and metabolic syndrome. *World J Gastroenterol.* 2009;15(15):1869-75.
53. Rosen ED, and Spiegelman BM. Adipocytes as regulators of energy balance and glucose homeostasis. *Nature.* 2006;444(7121):847-53.
54. Sun K, Tordjman J, Clement K, and Scherer PE. Fibrosis and adipose tissue dysfunction. *Cell Metab.* 2013;18(4):470-7.
55. Cancello R, Henegar C, Viguerie N, Taleb S, Poitou C, Rouault C, et al. Reduction of macrophage infiltration and chemoattractant gene expression changes in white adipose tissue of morbidly obese subjects after surgery-induced weight loss. *Diabetes.* 2005;54(8):2277-86.
56. Goossens GH, Bizzarri A, Venteclef N, Essers Y, Cleutjens JP, Konings E, et al. Increased adipose tissue oxygen tension in obese compared with lean men is accompanied by insulin resistance, impaired adipose tissue capillarization, and inflammation. *Circulation.* 2011;124(1):67-76.
57. Bel Lassen P, Charlotte F, Liu Y, Bedossa P, Le Naour G, Tordjman J, et al. The FAT Score, a Fibrosis Score of Adipose Tissue: Predicting Weight-Loss Outcome After Gastric Bypass. *J Clin Endocrinol Metab.* 2017;102(7):2443-53.
58. Marcelin G, Ferreira A, Liu Y, Atlan M, Aron-Wisnewsky J, Pelloux V, et al. A PDGFRalpha-Mediated Switch toward CD9(high) Adipocyte Progenitors Controls Obesity-Induced Adipose Tissue Fibrosis. *Cell Metab.* 2017;25(3):673-85.

59. Hughes VA, Roubenoff R, Wood M, Frontera WR, Evans WJ, and Fiatarone Singh MA. Anthropometric assessment of 10-y changes in body composition in the elderly. *Am J Clin Nutr.* 2004;80(2):475-82.
60. Fantin F, Di Francesco V, Fontana G, Zivelonghi A, Bissoli L, Zoico E, et al. Longitudinal body composition changes in old men and women: interrelationships with worsening disability. *J Gerontol A Biol Sci Med Sci.* 2007;62(12):1375-81.
61. Aguirre LE, Colleluori G, Fowler KE, Jan IZ, Villareal K, Qualls C, et al. High aromatase activity in hypogonadal men is associated with higher spine bone mineral density, increased truncal fat and reduced lean mass. *Eur J Endocrinol.* 2015;173(2):167-74.
62. Koutsari C, Ali AH, Nair KS, Rizza RA, O'Brien P, Khosla S, et al. Fatty acid metabolism in the elderly: effects of dehydroepiandrosterone and testosterone replacement in hormonally deficient men and women. *J Clin Endocrinol Metab.* 2009;94(9):3414-23.
63. Colleluori G, Chen R, Napoli N, Aguirre LE, Qualls C, Villareal DT, et al. Fat Mass Follows a U-Shaped Distribution Based on Estradiol Levels in Postmenopausal Women. *Front Endocrinol (Lausanne).* 2018;9:315.
64. Kotani K, Tokunaga K, Fujioka S, Kobatake T, Keno Y, Yoshida S, et al. Sexual dimorphism of age-related changes in whole-body fat distribution in the obese. *Int J Obes Relat Metab Disord.* 1994;18(4):207-2.
65. Colleluori G, Aguirre LE, Qualls C, Chen R, Napoli N, Villareal DT, et al. Adipocytes ESR1 Expression, Body Fat and Response to Testosterone Therapy in Hypogonadal Men Vary According to Estradiol Levels. *Nutrients.* 2018;10(9).
66. Cypess AM, Lehman S, Williams G, Tal I, Rodman D, Goldfine AB, et al. Identification and importance of brown adipose tissue in adult humans. *N Engl J Med.* 2009;360(15):1509-17.
67. Zingaretti MC, Crosta F, Vitali A, Guerrieri M, Frontini A, Cannon B, et al. The presence of UCP1 demonstrates that metabolically active adipose tissue in the neck of adult humans truly represents brown adipose tissue. *FASEB journal : official publication of the Federation of American Societies for Experimental Biology.* 2009;23(9):3113-20.
68. Eastment MC, Berry K, Locke E, Green P, O'Hare A, Crothers K, et al. BMI and Outcomes of SARS-CoV-2 Among US Veterans. *Obesity (Silver Spring).* 2021;29(5):900-8.
69. Kim SY, Yoo DM, Min C, Wee JH, Kim JH, and Choi HG. Analysis of Mortality and Morbidity in COVID-19 Patients with Obesity Using Clinical Epidemiological Data from the Korean Center for Disease Control & Prevention. *Int J Environ Res Public Health.* 2020;17(24).
70. Wang J, Zhu L, Liu L, Zhao XA, Zhang Z, Xue L, et al. Overweight and Obesity are Risk Factors of Severe Illness in Patients with COVID-19. *Obesity (Silver Spring).* 2020;28(11):2049-55.
71. O'Hearn M, Liu J, Cudhea F, Micha R, and Mozaffarian D. Coronavirus Disease 2019 Hospitalizations Attributable to Cardiometabolic Conditions in the United States: A Comparative Risk Assessment Analysis. *J Am Heart Assoc.* 2021;10(5):e019259.
72. Williamson EJ, Walker AJ, Bhaskaran K, Bacon S, Bates C, Morton CE, et al. Factors associated with COVID-19-related death using OpenSAFELY. *Nature.* 2020;584(7821):430-6.
73. Onder G, Palmieri L, Vanacore N, Giuliano M, Brusaferro S, and Italian National Institute of Health C-MG. Nonrespiratory Complications and Obesity in Patients Dying with COVID-19 in Italy. *Obesity (Silver Spring).* 2021;29(1):20-3.
74. Battisti S, Pedone C, Napoli N, Russo E, Agnoletti V, Nigra SG, et al. Computed Tomography Highlights Increased Visceral Adiposity Associated With Critical Illness in COVID-19. *Diabetes Care.* 2020;43(10):e129-e30.
75. Watanabe M, Caruso D, Tuccinardi D, Risi R, Zerunian M, Polici M, et al. Visceral fat shows the strongest association with the need of intensive care in patients with COVID-19. *Metabolism.* 2020;111:154319.

76. Petersen A, Bressem K, Albrecht J, Thiess HM, Vahldiek J, Hamm B, et al. The role of visceral adiposity in the severity of COVID-19: Highlights from a unicenter cross-sectional pilot study in Germany. *Metabolism.* 2020;110:154317.
77. Kompaniyets L, Goodman AB, Belay B, Freedman DS, Sucosky MS, Lange SJ, et al. Body Mass Index and Risk for COVID-19-Related Hospitalization, Intensive Care Unit Admission, Invasive Mechanical Ventilation, and Death - United States, March-December 2020. *MMWR Morb Mortal Wkly Rep.* 2021;70(10):355-61.
78. Morys F, and Dagher A. Poor Metabolic Health Increases COVID-19-Related Mortality in the UK Biobank Sample. *Front Endocrinol (Lausanne).* 2021;12:652765.
79. Thomas T, Stefanoni D, Reisz JA, Nemkov T, Bertolone L, Francis RO, et al. COVID-19 infection alters kynurenine and fatty acid metabolism, correlating with IL-6 levels and renal status. *JCI Insight.* 2020;5(14).
80. Nguyen M, Bourredjem A, Piroth L, Bouhemad B, Jalil A, Pallot G, et al. High plasma concentration of non-esterified polyunsaturated fatty acids is a specific feature of severe COVID-19 pneumonia. *Sci Rep.* 2021;11(1):10824.
81. Reiterer M, Rajan M, Gomez-Banoy N, Lau JD, Gomez-Escobar LG, Ma L, et al. Hyperglycemia in acute COVID-19 is characterized by insulin resistance and adipose tissue infectivity by SARS-CoV-2. *Cell Metab.* 2021;33(11):2174-88 e5.
82. Gupte M, Boustany-Kari CM, Bharadwaj K, Police S, Thatcher S, Gong MC, et al. ACE2 is expressed in mouse adipocytes and regulated by a high-fat diet. *Am J Physiol Regul Integr Comp Physiol.* 2008;295(3):R781-8.
83. Cinti S, Graciotti L, Giordano A, Valerio A, and Nisoli E. COVID-19 and fat embolism: a hypothesis to explain the severe clinical outcome in people with obesity. *Int J Obes (Lond).* 2020;44(8):1800-2.
84. Shin J, Toyoda S, Nishitani S, Fukuhara A, Kita S, Otsuki M, et al. Possible Involvement of Adipose Tissue in Patients With Older Age, Obesity, and Diabetes With Coronavirus SARS-CoV-2 Infection (COVID-19) via GRP78 (BIP/HSPA5): Significance of Hyperinsulinemia Management in COVID-19. *Diabetes.* 2021.
85. Hotamisligil GS. Inflammation, metaflammation and immunometabolic disorders. *Nature.* 2017;542(7640):177-85.
86. Talbot M, and Schemitsch EH. Fat embolism syndrome: history, definition, epidemiology. *Injury.* 2006;37 Suppl 4:S3-7.
87. Meng Y, Zhang M, Ling H, Huang S, Miao Q, Yu Y, et al. Nontraumatic Multiple-Organ Fat Embolism: An Autopsy Case and Review of Literature. *Am J Forensic Med Pathol.* 2020;41(2):131-4.
88. Fukumoto LE, and Fukumoto KD. Fat Embolism Syndrome. *Nurs Clin North Am.* 2018;53(3):335-47.
89. Gupta B, D'Souza N, Sawhney C, Farooque K, Kumar A, Agrawal P, et al. Analyzing fat embolism syndrome in trauma patients at AIIMS Apex Trauma Center, New Delhi, India. *J Emerg Trauma Shock.* 2011;4(3):337-41.
90. Bulger EM, Smith DG, Maier RV, and Jurkovich GJ. Fat embolism syndrome. A 10-year review. *Arch Surg.* 1997;132(4):435-9.
91. Hulman G. Fat macroglobule formation from chylomicrons and non-traumatic fat embolism. *Clin Chim Acta.* 1988;177(2):173-8.
92. Hulman G. Pathogenesis of non-traumatic fat embolism. *Lancet.* 1988;1(8599):1366-7.
93. Alexa AL, and Onutu AH. Fat Embolism Syndrome Mimicking a COVID-19 Infection. *Case Rep Crit Care.* 2021;2021:5519812.
94. ISS. Istituto Superiore di Sanità-Research ethics during the COVID-19 pandemic: observational and, in particular, epidemiological studies. 2020;47/2020.
95. Cinti S, Zingaretti MC, Cancello R, Ceresi E, and Ferrara P. Morphologic techniques for the study of brown adipose tissue and white adipose tissue. *Methods Mol Biol.* 2001;155:21-51.

96. de Wilde AH, Raj VS, Oudshoorn D, Bestebroer TM, van Nieuwkoop S, Limpens R, et al. MERS-coronavirus replication induces severe in vitro cytopathology and is strongly inhibited by cyclosporin A or interferon-alpha treatment. *J Gen Virol.* 2013;94(Pt 8):1749-60.
97. Alessandrini F, Caucci S, Onofri V, Melchionda F, Tagliabracci A, Bagnarelli P, et al. Evaluation of the Ion AmpliSeq SARS-CoV-2 Research Panel by Massive Parallel Sequencing. *Genes (Basel).* 2020;11(8).
98. Rodriguez AM, Elabd C, Amri EZ, Ailhaud G, and Dani C. The human adipose tissue is a source of multipotent stem cells. *Biochimie.* 2005;87(1):125-8.
99. Cummings BS, and Schnellmann RG. Measurement of cell death in mammalian cells. *Curr Protoc Pharmacol.* 2004;Chapter 12:Unit 12 8.
100. Camastra S, Vitali A, Anselmino M, Gastaldelli A, Bellini R, Berta R, et al. Muscle and adipose tissue morphology, insulin sensitivity and beta-cell function in diabetic and nondiabetic obese patients: effects of bariatric surgery. *Sci Rep.* 2017;7(1):9007.
101. Hirschbuhl K, Dintner S, Beer M, Wylezich C, Schlegel J, Delbridge C, et al. Viral mapping in COVID-19 deceased in the Augsburg autopsy series of the first wave: A multiorgan and multimethodological approach. *PLoS One.* 2021;16(7):e0254872.
102. Goldsmith CS, Tatti KM, Ksiazek TG, Rollin PE, Comer JA, Lee WW, et al. Ultrastructural characterization of SARS coronavirus. *Emerg Infect Dis.* 2004;10(2):320-6.
103. Ghadially F. *Ultrastructural Pathology of the Cell and Matrix.* 1997.
104. Perlman S, and Netland J. Coronaviruses post-SARS: update on replication and pathogenesis. *Nat Rev Microbiol.* 2009;7(6):439-50.
105. Lagana SM, Kudose S, Iuga AC, Lee MJ, Fazlollahi L, Remotti HE, et al. Hepatic pathology in patients dying of COVID-19: a series of 40 cases including clinical, histologic, and virologic data. *Mod Pathol.* 2020;33(11):2147-55.
106. Puray-Chavez M, LaPak KM, Schrank TP, Elliott JL, Bhatt DP, Agajanian MJ, et al. Systematic analysis of SARS-CoV-2 infection of an ACE2-negative human airway cell. *Cell Rep.* 2021;36(2):109364.
107. Konopka KE, Nguyen T, Jentzen JM, Rayes O, Schmidt CJ, Wilson AM, et al. Diffuse alveolar damage (DAD) resulting from coronavirus disease 2019 Infection is Morphologically Indistinguishable from Other Causes of DAD. *Histopathology.* 2020;77(4):570-8.
108. Cardinal-Fernandez P, Lorente JA, Ballen-Barragan A, and Matute-Bello G. Acute Respiratory Distress Syndrome and Diffuse Alveolar Damage. New Insights on a Complex Relationship. *Ann Am Thorac Soc.* 2017;14(6):844-50.
109. American Thoracic S, and European Respiratory S. American Thoracic Society/European Respiratory Society International Multidisciplinary Consensus Classification of the Idiopathic Interstitial Pneumonias. This joint statement of the American Thoracic Society (ATS), and the European Respiratory Society (ERS) was adopted by the ATS board of directors, June 2001 and by the ERS Executive Committee, June 2001. *Am J Respir Crit Care Med.* 2002;165(2):277-304.
110. Wellman TJ, de Prost N, Tucci M, Winkler T, Baron RM, Filipczak P, et al. Lung Metabolic Activation as an Early Biomarker of Acute Respiratory Distress Syndrome and Local Gene Expression Heterogeneity. *Anesthesiology.* 2016;125(5):992-1004.

Table 1. Characteristics of each subject included in the study.

N	ID	SARS-CoV-2 by RT-PCR	BMI (kg/m^2)	Gender	Age	HPB	T2DM	CVD	PRE-EXISTING RESPIRATORY COMORBIDITIES	CAUSES OF DEATH
1	34-18	-	28.04	M	48	+	-	+	-	Multiple Organ Dysfunction Syndrome (MODS)
2	48-19	-	24.2	M	74	-	-	-	+	Respiratory failure
3	44/20	+	29.3	F	62	+	-	-	+	Cardiac rhythm and/or conduction disease following right myocardial infarction
4	45/20	+	31.0	M	67	-	+	-	-	Respiratory failure
5	50/20	+	29.0	F	70	-	-	-	-	Respiratory failure
6	52/20	+	31.2	M	67	-	-	-	-	Respiratory failure
7	56/20	+	31.0	M	92	+	-	-	+	Respiratory failure in a setting of pre-existing comorbidities
8	67/20	-	29.1	F	63	-	-	-	-	Cardiac rhythm and/or conduction disease
9	74/20	-	27,3	F	67	+	+	-	-	Respiratory failure following pleural empyema
10	75/20	-	27.5	M	58	+	-	+	-	Cardiac rhythm and/or conduction disease
11	78/20	-	30.4	M	55	-	-	+	-	Cardiac rhythm and/or conduction disease
12	82/20	-	20.9	M	55	-	-	-	-	Cardiac rhythm and/or

										conduction disease
13	81/20	-	16.0	M	27	-	-	-	-	Lymphoma
14	129-20	-	29.4	M	63	-	-	-	-	Respiratory depression following acute drug intoxication
15	131-20	+	30.1	M	70	-	-	-	+	Respiratory failure
16	133-20	-	29.3	M	72	-	-	-	-	Cranio-encephalic trauma following accidental fall
17	144-20	+	28.0	F	83	-	+	-	-	Respiratory failure
18	146-20	+	31.1	M	56	-	+	-	-	Respiratory failure
19	147-20	+	27.3	F	60	-	+	-	-	Respiratory failure
20	148-20	+	24.0	F	82	-	-	-	+	Respiratory failure
21	150-20	-	28.5	F	53	-	-	-	-	Cardiac rhythm and/or conduction disease
22	152-20	+	29.4	M	51	-	+	-	-	Respiratory failure and cardio-circulatory arrest. Patient treated with ECMO
23	154-20	-	31.8	M	75	-	-	+	-	Cardiac rhythm and/or conduction disease
24	155-20	-	29.4	F	44	-	-	+	+	Cardio-circulatory arrest in pneumonia and

										metapneumonic pleurisy
25	156-20	-	31.2	F	39	-	-	-	-	Cardiac rhythm and/or conduction disease
26	162-20	-	35.5	M	43	-	-	-	-	Cardiac rhythm and/or conduction disease
27	00-21	+	22.8	M	76	-	-	-	+	Respiratory failure
28	0-21	+	46.7	M	66	+	-	-	+	Respiratory failure
29	8-21	-	27.7	M	72	+	+	+	-	Cardiac rhythm and/or conduction disease
30	11-21	-	30.4	M	72	+	+	+	-	Cardiac rhythm and/or conduction disease
31	13-21	-	28.3	M	55	-	-	+	-	Cardiac rhythm and/or conduction disease
32	17-21	-	21.2	M	90	+	+	-	+	Cardio-circulatory arrest in pneumonia and rectal cancer
33	28-21	+	32.0	F	80	+	-	+	-	Respiratory failure
34	31-21	+	36.0	M	56	+	-	-	-	Respiratory failure
35	32-21	+	23.6	M	77	+	-	+	+	Respiratory failure
36	33-21	-	45.7	M	48	-	-	+	-	Cardiac rhythm and/or conduction disease

37	35-21	-	23.4	M	79	-	-	+	-	Carbon monoxide intoxication
38	36-21	-	25.0	M	55	-	-	+	+	Cardiac rhythm and/or conduction disease
39	21/15	+	29.4	F	71	-	+	-	-	Respiratory failure
40	38-21	+	28.4	F	53	-	-	-	-	Respiratory failure
41	55/20	-	26.3	F	58	+	-	-	-	Cardiac rhythm and/or conduction disease
42	03/20	+	30.0	M	73	-	-	-	-	Respiratory failure

Positive symbol indicates presence; negative symbol indicates absence. BMI=Body Mass Index; HBP= High blood pressure; T2DM: Type 2 Diabetes Mellitus; CVD: Cardiovascular disease which includes: cardiopathy, myocardiosclerosis; pre-existing respiratory comorbidities include: bacterial pneumonia, mesothelioma, amyloidosis; ECMO= Extracorporeal membrane oxygenation.

Table 2. Prevalence of respiratory conditions, type 2 diabetes, hypertension, and cardiovascular diseases in the study population.

	Controls (n:23)	**COVID-19 (n:19)**	**p**
Respiratory conditions*; n (%)	5 (21.7)	10 (52.6)	0.03
Type 2 Diabetes; n (%)	5 (21.7)	6 (31.6)	0.47
Hypertension; n (%)	9 (39)	7 (36)	0.87
Cardiovascular disease; n (%)	8 (34.7)	2 (10.5)	0.06
*Pneumonia, dyspnoea, respiratory distress			